AD-A100 471 YALE UNIV NEW HAVEN CONN DEPT OF ENGINEERING AND AP--ETC F/G 20/5
WAVE-PARTICLE INTERACTION ON RELATIVISTIC ELECTRON BEAMS.(U)
JUN 81 I B BERNSTEIN, J L HIRSHFIELD N00014-79-C-0588

UNCLASSIFIED NL

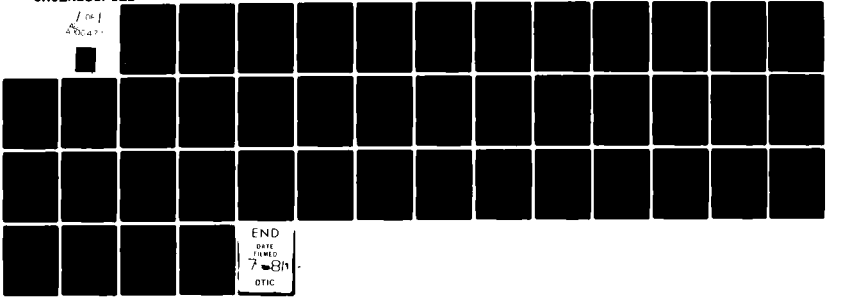

END
DATE FILMED
7-81
DTIC

UNCLASSIFIED

SECURITY CLASSIFICATION OF THIS PAGE (When Data Entered)

LEVEL III

REPORT DOCUMENTATION PAGE

READ INSTRUCTIONS BEFORE COMPLETING FORM

1. REPORT NUMBER	2. GOVT ACCESSION NO.	3. RECIPIENT'S CATALOG NUMBER
3-4	AD-A100471	

4. TITLE (and Subtitle)

Wave-Particle Interaction on Relativistic Electron Beams

5. TYPE OF REPORT & PERIOD COVERED

Summary 6/1/80-6/1/81

6. PERFORMING ORG. REPORT NUMBER

3-4

7. AUTHOR(s)

Ira B. Bernstein and J. L. Hirshfield

8. CONTRACT OR GRANT NUMBER(s)

N00014-79-C-0588

9. PERFORMING ORGANIZATION NAME AND ADDRESS

Yale University
Department of Engineering & Applied Science
New Haven, CT 06520

10. PROGRAM ELEMENT, PROJECT, TASK AREA & WORK UNIT NUMBERS

NR 020-043

11. CONTROLLING OFFICE NAME AND ADDRESS

Office of Naval Research, Physics Program Code 421
800 N. Quincy Street
Arlington, VA 22217

12. REPORT DATE

June 15, 1981

13. NUMBER OF PAGES

43

14. MONITORING AGENCY NAME & ADDRESS (if different from Controlling Office)

15. SECURITY CLASS. (of this report)

Unclassified

15a. DECLASSIFICATION/DOWNGRADING SCHEDULE

16. DISTRIBUTION STATEMENT (of this Report)

Approved for public release; distribution unlimited.

17. DISTRIBUTION STATEMENT (of the abstract entered in Block 20, if different from Report)

18. SUPPLEMENTARY NOTES

19. KEY WORDS (Continue on reverse side if necessary and identify by block number)

Free Electron Laser
Relativistic Beam Plasma Interaction

DTIC ELECTED JUN 23 1981 S G

20. ABSTRACT (Continue on reverse side if necessary and identify by block number)

DD FORM 1 JAN 73 1473 EDITION OF 1 NOV 65 IS OBSOLETE S/N 0102-014-6601

UNCLASSIFIED

SECURITY CLASSIFICATION OF THIS PAGE (When Data Entered)

AD A100471

DTIC FILE COPY

81 6 23 021

Wave Particle Interactions on Relativistic Electron Beams

Principal Investigators: Ira B. Bernstein and J. L. Hirshfield
Yale University
Department of Engineering & Applied Science
P.O. Box 2159, Yale Station
New Haven, CT 06520
Ref: Contract N00014-79-0-0588

Papers Prepared for Publication: (copies attached)

1. "Free-Electron Laser with a Strong Axial Magnetic Field," L. Friedland and J. L. Hirshfield, Phys. Rev. Lett. 44, 1456 (1980).

2. "Electron Beam Dynamics in Combined Guide and Pump Magnetic Fields for Free Electron Laser Applications," L. Friedland, Phys. Fluids 23, 2376 (1980).

3. "Theory of the Free Electron Laser in Combined Helical Pump and Axial Guide Fields," I. B. Bernstein and L. Freidland, Phys. Rev. A 23, 816 (1981).

4. "Orbit Stability in Free Electron Lasers," P. Avivi, F. Dothan, A. Fruchtman, A. Ljudmirsky, and J. L. Hirshfield, to be published in International Journal Infrared and Millimeter Waves.

5. "Degradation in Gain for a Free Electron Laser Amplifier Due To Electron Momentum Spread," A. Fruchtman and J. L. Hirshfield, to be published in International Journal Infrared and Millimeter Waves.

Personnel

Yale University:

Ira B. Bernstein, Professor of Applied Science
Jay L. Hirshfield, Professor of Applied Science
Lazar Friedland, Assistant Professor of Applied Science
Soo Yong Park, Visiting Research Scholar (B-K Dynamics-NRL)
Ralph A. Smith, Undergraduate Research Aide

Hebrew University:

P. Avivi, Associate Professor of Physics
F. Dothan, Associate Professor of Physics
A. Ljudmirsky, Research Staff Physicist
J. Schmulovitch, Research Staff Physicist
A. Fruchtman, Research Assistant

Other Government Sponsored Research with which Principal Investigators are associated.

Jay L. Hirshfield: Research on Gyrotrons
ONR Contract N00014-80-C-0075
$299,892 Oct. 1, 1980 - Sep. 30, 1981

Electromagnetic Isotope Separation in Laser-Initiated Vacuum Arcs
NSF Grant CPE-7916500
$62,322 June 30, 1981 - June 30, 1982

Ira B. Bernstein: Topics in Theoretical Plasma Physics
NSF Grant PHY78-08443
Dec. 31, 1980 - Dec. 31, 1981
$25,775

Theoretical and Numerical Studies in Magnetic Mirror Fusion
DOE Contract DE-AC02 77ET53057
Nov. 1, 1980 - Oct. 31, 1981
$92,000

SUMMARY OF SCIENTIFIC PROGRESS TO DATE

Here brief summaries are given for topics where significant progress has been achieved, but where as yet no papers have been prepared for publication.

1. Non-Linear Theory (I. B. Bernstein and L. Friedland)

The non-linear theory of a steady state free electron laser amplifier consisting of a relativistic electron beam in helical pump and axial confining magnetic fields illuminated by monochromatic radiation has been formulated. The introduction of Lagrangian variables permits an exact integration of the continuity equation to express the current density at a general field point in terms of the current density at injection and the velocity at the field point in question. The axial electric field is found in a similar way by integrating Poisson's equation. The parallel momentum equation is reduced to an ordinary differential equation and permits the electron orbits to turn in the wave frame, corresponding as one advances along the beam in the direction of propagation to the development of multistreaming. The reduced equations, and the coupled wave equations for the transverse vector potential are being analyzed, and suitable numerical methods for their solution are being determined. Preliminary numerical studies have begun.

2. Quasi-Linear Theory (I. B. Bernstein and L. Friedland)

A quasi-linear theory of the steady free electron laser amplifier consisting of a helical pump and relativistic electron beam illuminated by a monochromatic wave has been formulated. A linearized WKB description is employed to describe the electromagnetic field, and the steady state density, mean velocity, etc. are determined correct to second order in the high frequency amplitude. The helical pitch is allowed to vary with position so as to keep the system in a configuration of maximum gain as the beam decelerates on converting its energy into radiation. The analysis of the results is continuing, numerical studies are underway, and a preliminary manuscript has been prepared.

3. Exact Magnetic Fields of a Bifilar Helix (S. Y. Park, R. A. Smith, and J. L. Hirshfield)

The static magnetic field of a bifilar helix has been derived exactly. The components B_1, B_2, and B_3 have each been determined as functions of r, and θ-kz, where $2\pi/k$ is the period of the double helix, and where ($\hat{e}_1$, $\hat{e}_2$, $\hat{e}_3$) is the basis vector set dictated by helix symmetry. In usual FEL theory $B_1 = B_3 = 0$, and $B_2 = \text{const}$. The theory developed here gives, for a helix of specified radius and period, the radial beam positions for which the usual assumption is valid. Higher order multi-pole fields are significant off axis, where annular beams are commonly placed.

4. Non-Helical Orbits in a Free Electron Laser (S. Y. Park, R. A. Smith and J. L. Hirshfield)

An exact analytic solution has been found for the orbit of a charged particle moving in the combined magnetic field of a bifilar helical wiggler

and a uniform solenoid. The axial velocity is shown to satisfy an anharmonic oscillator equation whose solutions are Jacobian elliptic functions. Other velocity components are readily determined from the axial velocity. Solutions are classified according to the type of Jacobian elliptic function, which in turn is determined by magnetic field parameters and initial particle conditions. This exact solution is to be used to calculate the spectrum of single-particle spontaneous emission; significant emission at harmonic wavelengths is indicated.

5. Electron Beam Analyzer (P. Avivi, F. Dothan, A. Fruchtman, and J. L. Hirshfield)

Electromagnetic gain in a FEL is a sensitive function of the momentum distribution of the beam electrons. The physical mechanism which dominates the gain process may even change as one goes from a "cold" beam to a beam with a finite skewed spread in momentum. It is thus crucial to measure the momentum distribution of the electron beam in a FEL in order to interpret the results. With this in mind we have designed a 90° magnetic deflection analyzer which is capable of determining average electron momentum and relative distribution of momentum, for a small sample of the beam. At a deflection angle of 90° the analyzer's dispersion is a maximum; momentum resolution of 0.1% appears possible. This analyzer is now under construction, in two stages. In the first stage, about to be installed, the analyzer responds in a single channel (i.e., in a single momentum bin) on each accelerator shot. In the second stage, a multichannel collector and readout will be possible on each shot.

6. Operation of Febetron Accelerator (A. Ljudmirsky, J. Smulovits, F. Dothan, H. Sharon, and J. L. Hirshfield)

The $\sim$ 400 keV Febetron accelerator has been successfully operated in the magnetic field and vacuum tank in which the free electron laser experiments are to be conducted. The manufacturer's Blumlein pulse line has been removed so that the 50 nsec Marks bank is terminated directly by the foilless field emission diode. Diode impedance is adjusted, both empirically and with the guidance of the NRL experience, by shaping the cathode stem and the anode geometry. Stable beams in the current range 100-1000 A have been successfully generated and launched along the full axis of the combined guide and wiggler magnetic fields of the device. Electromagnetic radiation and gain measurements at 35 GHz are about to begin.

Free-Electron Laser with a Strong Axial Magnetic Field

L. Friedland and J. L. Hirshfield
Department of Engineering and Applied Science, Mason Laboratory, Yale University, New Haven, Connecticut 06520
(Received 27 February 1980)

A small-signal theory is given for gain in a free-electron laser comprising a cold relativistic electron beam in a helical periodic transverse, and a strong uniform axial, magnetic field. Exact finite-amplitude, steady-state helical orbits are included. If perturbed, these orbits oscillate about equilibrium, so that substantial gain enhancement can occur if the electromagnetic perturbations resonate with these oscillations. This gain enhancement need not be at the cost of frequency upshift.

PACS numbers: 42.55.-f, 41.70.+t, 41.80.Dd

Intensive activity is underway to exploit the gain properties of a relativistic electron beam undulating in a periodic transverse magnetic field. Such free-electron laser (FEL) configurations have provided oscillation at 3.4 (Ref. 1) and 400 μm,[2] and amplification at 10.6 μm.[3] Theory has advanced apace,[4] and elaborate schemes have been proposed for obtaining high FEL efficiency.[5] A factor which limits the practical application of this interaction at wavelengths shorter than perhaps a few microns is the rapid decrease in small-signal gain G_0 as the electron energy increases. This is shown explicitly in the well-known result[6] for G_0 in the single-particle limit (i.e., when collective effects are negligible)

$$G_0 = (\omega_p \xi/k_0 c)^2 (k_0 L/2\gamma)^3 F'(\theta). \quad (1)$$

Here ω_p and γ are the beam plasma frequency $Ne^2/m\epsilon_0$ and normalized energy W/mc^2, k_0 and ξ are the helical transverse magnetic field wave number $2\pi/l$ and normalized strength $eB_\perp/mck_0$, L is the interaction length, and $F'(\theta) = (d/d\theta)(\sin\theta/\theta)^2$ is the line-shape factor, with $\theta = [k_0 v_{30} - \omega(1 - v_{30}/c)](L/2c)$, where v_{30} is the unperturbed electron axial velocity. The peak gain occurs at $\theta = 1.3$, where $F'(\theta) = 0.54$. For example, with γ

$=10$, $l=1.05$ cm, $\omega_p=5\times10^7$ sec^{-1}, $\xi=1$ ($B_\perp=10.2$ kG), and $L=130$ cm, the peak gain is $G_{0p}=0.002\,47$ at a wavelength of 105 μm. For $\gamma=100$, $l=10.5$ cm, $\omega_p=2\times10^9$ sec^{-1}, $\xi=1$ ($B_\perp=1.02$ kG), and $L=260$ cm, the peak gain is $G_{0p}=0.003\,16$ at a wavelength of 10.5 μm. These gain values may be large enough to sustain oscillations if highly reflecting mirrors are judiciously added but the strong helical fields required (particularly the 10.2-kG case) may be beyond the capability of present superconducting coil technology.[7]

A suggestion has appeared for enhancing the small-signal gain above values given by Eq. (1) (or for achieving comparable gains with smaller $B_\perp$) by employing a strong axial magnetic field so as to exploit resonance between the cyclotron frequency and the undulatory frequency.[8] The present Letter presents a single-particle derivation for the small-signal gain of a FEL in a uniform axial magnetic field B_0. We shall demonstrate that careful adjustment of the system parameters will allow enhancement of the FEL small-signal gain by an order of magnitude or more (for the above examples) *without increasing the undulatory velocity*. This result goes beyond that predicted by Sprangle and Granatstein[8] who have suggested that the only effect of the axial magnetic field would be to add a multiplicative factor $(1-\Omega/k_0c\gamma)^{-2}$ to Eq. (1), due to the aforementioned resonance giving an enhanced undulatory velocity $v_\perp$, where $\Omega=eB_0/m$. This result is in fact predicted by our analysis as a limiting case. Of course, any mechanism which increases the undulatory velocity $v_\perp$ would increase the gain, but this would also reduce the relativistic frequency upshift, since

$$\omega\simeq k_0c(1-v_{30}/c)^{-1}=2\gamma^2k_0c(1+\gamma^2v_\perp^2/c^2)^{-1}.$$

If, for example, $\gamma v_\perp/c=1$ without the axial magnetic field, then a given gain enhancement η achieved through this resonance alone would result in a reduction in frequency upshift by a factor $(1+\eta)/2$. The process we describe in this Letter will be shown to permit significant gain enhancement without undue sacrifice in frequency upshift. The gain enhancement originates when the electromagnetic perturbations resonate with the natural frequency of oscillation of electrons on finite amplitude equilibrium helical orbits. Prior workers have not considered this effect.

A full derivation of our result will be presented elsewhere.[9] Exact unperturbed relativistic orbits are considered in the customary FEL model magnetic field

$$\vec{B}(\vec{r})=B_0\hat{e}_z+B_\perp(\hat{e}_x\cos k_0z+\hat{e}_y\sin k_0z). \tag{2}$$

These orbits, which have been the subject of recent study,[10] can possess more than one steady state, depending upon γ, B_0, $B_\perp$, and k_0. These steady states are characterized by the normalized velocity components (i.e., $u_i=v_i/c$)

$$u_{10}=0,\quad u_{20}=k_0\xi u_{30}/(k_0u_{30}\gamma-\Omega/c),$$
$$u_{30}=(1-u_{20}^2-\gamma^{-2})^{1/2}, \tag{3}$$

where the basis vectors $\hat{e}_1(z)=-\hat{e}_x\sin k_0z+\hat{e}_y\cos k_0z$, $\hat{e}_2(z)=-\hat{e}_x\cos k_0z-\hat{e}_y\sin k_0z$, and $\hat{e}_3(z)=\hat{e}_z$ have been introduced to track the symmetry of the transverse magnetic field. Figure 1 shows u_{30} vs Ω/c for $k_0=6.0$ cm^{-1}, $\xi=1.0$, and $\gamma=10$. For $\Omega>\Omega_{cr}\equiv k_0c[(\gamma^2-1)^{1/3}-\xi^{2/3}]^{3/2}$, it is seen that only one branch exists (branch C). But for $\Omega<\Omega_{cr}$ two additional branches (A and B) are allowed: Branch B has been shown to be unstable, in that the orbits exhibit nonhelical, highly anharmonic motions, while branches A and C have orderly helical orbits. Stability is insured if $\mu^2\equiv a^2-bd>0$, where $a=k_0cu_{30}\xi/\gamma u_{20}$, $b=\Omega u_{20}/\gamma u_{30}$, and $d=k_0c\xi/\gamma$. The quantity μ is the natural resonance frequency in response to small perturbations of the orbit: We shall show that strong resonance response of the electrons to electromagnetic perturbation can lead to enhanced FEL gain for small μ, i.e., for Ω close to Ω_{cr}.

The derivation of FEL gain proceeds by solving the single-particle equations of motion, subject to weak electromagnetic perturbing fields $\vec{E}=\hat{e}_xE_0\cos(kz-\omega t)$ and $\vec{B}=\hat{e}_y(kc/\omega)E_0\cos(kz-\omega t)$,

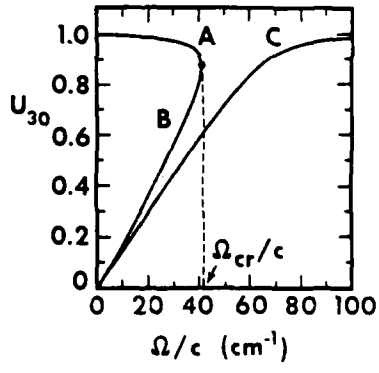

FIG. 1. Steady-state normalized axial velocity u_{30} as a function of normalized axial magnetic field Ω/c. For this example $k_0=6.0$ cm^{-1}, $\xi=1.0$, and $\gamma=10$. Gain enhancement discussed in this work is for orbits on either branch A or branch C.

about the equilibrium orbits on either branch A or C as discussed above. These equations are

$$\dot{u}_1 = (k_0 c u_3 - \Omega/\gamma)u_2 - (k_0 c\xi/\gamma)u_3 - (\dot{\gamma}/\gamma)u_1 + (eE_1/mc\gamma)(kcu_3/\omega - 1), \tag{4}$$

$$\dot{u}_2 = -(k_0 c u_3) - \Omega/\gamma)u_1 - (\dot{\gamma}/\gamma)u_2 + (eE_2/mc\gamma)(kcu_3/\omega - 1), \tag{5}$$

$$\dot{u}_3 = (k_0 c\xi/\gamma)u_1 + (kc/\omega - u_3)(\dot{\gamma}/\gamma), \tag{6}$$

where $\dot{\gamma} = -(e/mc)(u_1E_1 + u_2E_2)$ and

$$2(E_2 + iE_1) = -E_0 \exp\{i[(k_0 + k)u_3 ct - \omega t + \alpha]\}$$

with α the random initial electron phase. When time variations and electromagnetic fields are absent, Eqs. (4)–(6) lead to the exact steady states given by Eq. (3). To linearize Eqs. (4)–(6), we introduce the velocity perturbations $w_i = u_i - u_{i0} \ll u_{i0}$ and retain only the lowest-order quantities. This results in $\ddot{w}_1 + \mu^2 w_1 = AE_0 \cos(\beta t + \alpha)$, or

$$w_1 = \frac{AE_0}{\mu^2 - \beta^2}[\cos(\beta t + \alpha) - \cos\mu t \cos\alpha + (\beta/\mu)\sin\mu t \sin\alpha] + \mu^{-1}\dot{w}_1(0)\sin\mu t, \tag{7}$$

where

$$A = (a + \beta)(1 - u_{30}) + bu_{20}, \quad \beta = c(k + k_0)u_{30} - \omega, \quad \omega \simeq kc, \quad \dot{w}_1(0) = (eE_0/2\gamma mc)(1 - u_{30})\sin\alpha,$$

and $w_1(0) = 0$. The other components follow from

$$\dot{w}_2 = -aw_1 + (eE_0/2mc\gamma)(1 - u_{30} - u_{20}^2)\cos(\beta t + \alpha), \quad w_2(0) = 0; \tag{8}$$

and

$$\dot{w}_3 = dw_1 + (eE_0/2mc\gamma)u_{20}(1 - u_{30})\cos(\beta t + \alpha), \quad w_3(0) = 0. \tag{9}$$

Equation (7) for w_1 exhibits the aforementioned natural resonance at frequency μ, while the electromagnetic perturbation drives the transverse motion at frequency β. Gain enhancement can be expected when μ is close to β.

The energy gain for an electron is calculated from $(mc/e)d\gamma/dt \simeq -w_1E_{10} - w_2E_{20} - u_{20}E_{21}$. The first-order variation in electric field E_{21} originates from small phase variations as u_3 changes. Thus this becomes

$$(mc/e)d\gamma/dt = -w_1E_{10} - w_2E_{20} - \tfrac{1}{2}E_0(k + k_0)cu_{20}\sin(\beta t + \alpha)\int_0^t dt' w_3(t'). \tag{10}$$

The third term in Eq. (10) is much larger than the other two on account of the factor $k + k_0$. The dominant single-particle energy transfer in the FEL (even with an axial magnetic field) is seen to be by work ecu_2E_2 done along the transverse undulatory motion, enhanced by the strong variation in E_2 as its phase varies through w_3. The energy variation [Eq. (10)] is averaged over random phase α to give $\langle d\gamma/dt\rangle$, which in turn leads to the gain through $G = 2(\epsilon_0 E_0^2)^{-1}Nmc^2\int_0^T dt\langle d\dot{\gamma}/dt\rangle$, where N is the beam electron density and $T = L/c$ is the total interaction time for the electrons in a system of length L.

The final result is

$$G = \frac{\omega_p^2 k_0 c}{16\gamma}u_{20}^2 T^3\left\{\left[1 + \frac{a}{\mu_2}\left(a + \beta + \frac{u_{20}b}{1 - u_{30}}\right)\right]\left[F'(\theta) - \frac{F(\theta + \varphi) - F(\theta - \varphi)}{2\varphi}\right] + \frac{F(\theta + \varphi) - F(\theta - \varphi)}{2\varphi} - \frac{a}{\mu^2 T}\left[P'(\theta) - \frac{P(\theta + \varphi) - P(\theta - \varphi)}{2\varphi}\right]\right\}, \tag{11}$$

where $\theta = \beta T/2$, $\varphi = \mu T/2$, $F(x) = (\sin x/x)^2$, and $P(x) = xF(x)/2$; and where we have approximated $(k + k_0)(1 - u_{30}) \simeq k_0$. We shall examine Eq. (11) in several limits.

For $\mu \gg \beta$, only the terms involving $F'(\theta)$ and $P'(\theta)$ in Eq. (11) are significant, and on branch A the latter of these is smaller than the former by at least a factor 2φ. Thus to a good approximation we may write

$$G(\mu \gg \beta) = Z(\omega_p^2/16\gamma)k_0 c u_{20}^2 T^3 F'(\theta), \tag{12}$$

where $Z = 2 + \mu^{-2}[a\beta + bd(1 - u_{30})^{-1}]$. In the case where the axial magnetic field is absent, $\Omega = 0$, $\mu = a = k_0 c u_{30} \gg \beta$, and $u_{20} = \xi/\gamma$. Thus, $Z \simeq 2$ and Eq. (12) goes over to Eq. (1). When $\Omega \neq 0$ and μ

$\gg \beta$, gain enhancement can be achieved as claimed by the prior workers,[8] due to resonant enhancement of u_{20}, but not without sacrificing frequency upshift, as discussed above.

However a more attractive possibility exists when μ is small, and approaches β. Here one can approximate $Z \simeq \mu^{-2} bd(1-u_{30})^{-1} \gg 1$; this results from resonance between the electromagnetic perturbation which gives oscillatory motion to the electron at a frequency β, close to its natural oscillation frequency μ. Gain enhancement due to large Z is seen to be possible without simultaneously increasing u_{20}, so that the desirable frequency upshift property of the FEL need not be sacrificed.

We define a gain enhancement factor $\eta = G/G_0$ to compare two free-electron lasers, identical except that one has a strong axial magnetic field, while the second does not. In the first laser, the transverse magnetic field $B_\perp$ is reduced so that u_{20} is the same for both lasers. (This assures that both enjoy the same frequency upshift.) Then

$$\eta = Z\{1 - [F(\theta+\varphi) - F(\theta-\varphi)]/2\varphi F'(\theta)\}. \quad (13)$$

We have evaluated Eq. (13) for two examples with the parameters cited in the first paragraph of this Letter, holding $|\theta| = 1.3$ where $|F'(\theta)|$ has its maximum value. The results are shown in Fig. 2 for the $\gamma = 10$ example. In Fig. 2(a) we plot the gain enhancement factor η as a function of the transverse magnetic field normalized strength ξ for the FEL with the axial guide magnetic field. The solid curves are for steady-state orbits on branch C; the dashed curves for branch A. On branch A, gain occurs for $\theta > 0$, while on branch C gain occurs for $\theta < 0$. Two transverse magnetic fields for the FEL without axial field corresponding to $\xi_0 = 1$ and 0.5 are shown. Figure 2(b) shows the required values of axial guide field. One sees a gain enhancement of 31 (on branch C) at $\xi = 5 \times 10^{-3}$ for an axial guide field of 102 kG. The transverse magnetic field required is reduced to 51 G, and the gain is increased to 0.0766 at $\lambda = 105$ μm. Higher gain is predicted on branch A. For the $\gamma = 100$ example at $\lambda = 10.5$ μm, we find a gain enhancement of 16 (on branch A) at $\xi = 3 \times 10^{-2}$ for an axial guide field of 99.5 kG. The transverse magnetic field required is reduced to 30.6 G, and the gain is increased to 0.0506.

Of course when the predicted single-pass gain is large (say > 0.1) this theory must be modified. Furthermore, finite electron momentum spread (neglected here) will mitigate against gain, as for a FEL without a guide field. These effects deserve careful study. However, to the extent that these effects are negligible, our theory shows that provision of a strong uniform axial magnetic field can allow significant small-signal gain enhancement, and significant reduction in the required transverse magnetic field strength in a FEL, without undue compromise in operating frequency below that given by the idealized upshift value $2\gamma^2 k_0 c$.

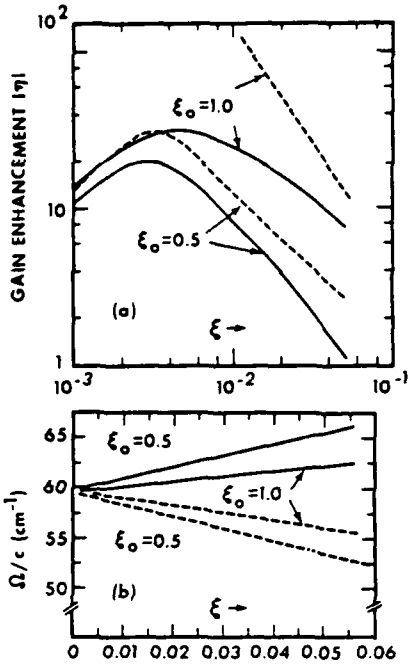

FIG. 2. (a) Gain enhancement $|\eta|$ and (b) corresponding normalized axial magnetic field Ω/c, vs transverse magnetic field parameter ξ. The values $\xi_0 = 0.5$ and 1.0 are for the FEL without axial field, and provide the same u_{20} as do the indicated (smaller) values of ξ for the FEL with the indicated axial field strength. Example is for $\gamma = 10$, $k_0 = 6.0$ cm^{-1}, and $L = 130$ cm. Solid curves, orbits on branch C; dashed curves, orbits on branch A. For high enhancement values, such as on the $\xi_0 = 1.0$ branch A example, the numerical precision required to compute accurate results suggests that the phenomenon is very sensitive to the system parameters.

This work was supported in part by the U. S. Office of Naval Research and in part by the U. S. Air Force Office of Scientific Research.

[1] L. R. Elias, W. M. Fairbank, J. M. J. Madey, H. A. Schwettman, and T. I. Smith, Phys. Rev. Lett. 36, 717 (1976).

[2]D. B. McDermott, T. C. Marshall, and S. P. Schlesinger, Phys. Rev. Lett. 41, 1368 (1978).

[3]D. A. G. Deacon, L. R. Elias, J. M. J. Madey, G. J. Ramian, H. A. Schwettman, and T. I. Smith, Phys. Rev. Lett. 38, 892 (1977).

[4]I. B. Bernstein and J. L. Hirshfield, Phys. Rev. Lett. 40, 761 (1978); T. Kwan and J. M. Dawson, Phys. Fluids 22, 1089 (1979); I. B. Bernstein and J. L. Hirshfield, Phys. Rev. A 20, 1661 (1979); P. Sprangle and R. A. Smith, Phys. Rev. A 21, 293 (1980).

[5]P. Sprangle, C.-M. Tang, and W. M. Manheimer, Phys. Rev. A 21, 302 (1980).

[6]W. B. Colson, *Physics of Quantum Electronics* (Addison-Wesley, Reading, Mass., 1977), Vol. 5.

[7]J. P. Blewett and R. Chasman, J. Appl. Phys. 48, 2692 (1977).

[8]P. Sprangle and V. L. Granatstein, Phys. Rev. A 17, 1792 (1978).

[9]L. Freidland and J. L. Hirshfield, to be published.

[10]L. Friedland, to be published.

Electron beam dynamics in combined guide and pump magnetic fields for free electron laser applications

L. Friedland

Department of Computer Science, Yale University, New Haven, Connecticut 06520
(Received 13 December 1979; accepted 21 August 1980)

The propagation of a cold relativistic electron beam in a free electron laser with an axial guide magnetic field is considered. The possibility of several steady-state helical trajectories for the electrons is shown, and the stability against perturbations and accessibility of such steady states is considered. Necessary and sufficient conditions for the stability are derived and indicate the importance of the transition region at the entrance of the laser. Possible modes of operation of the laser in different steady-state regimes are suggested and illustrated by numerical examples.

I. INTRODUCTION

The propagation of a relativistic electron beam in transverse periodic magnetic structures has been studied extensively in recent years. These studies were stimulated by the first experimentally successful free electron laser[1] which confirmed the theoretically predicted[2] possibility of using the energy stored in the relativistic beam as a source of short wavelength coherent radiation.

The most frequently used periodic magnetic pump field in a free electron laser is the transverse field produced on the axis of a double helical current winding with equal and opposite currents in each helix (a device usually referred to as a magnetic wiggler). The unperturbed motion of the electrons of the beam in the wiggler is quite simple. The reason for simplicity is that the magnetic field on the axis of a wiggler can be approximately described by a transverse vector potential $\mathbf{A}_\perp(z)$, depending only on the distance z along the axis. Therefore, the canonical transverse momentum $\mathbf{P}_\perp = \gamma m \mathbf{v}_\perp - (e/c)\mathbf{A}_\perp$ of an electron is a constant of motion,[3] which with the conservation of energy $\gamma = [1 - (v_\perp/c)^2 - (v_\parallel/c)^2]^{-1/2} = \text{const}$, uniquely defines the perpendicular and parallel components $\mathbf{v}_\perp$ and $\mathbf{v}_\parallel$ of the velocity of the electrons in the beam, for a given assignment of $\mathbf{A}_\perp(z)$. It can now be easily shown[4] that the electrons in a magnetic wiggler have helical trajectories with the same period as that of the wiggler. This simple model of the motion has been exploited in many theoretical studies, describing the operation and parametric behavior of the free electron laser.[5]

In all experiments, however, there is also an axial guide magnetic field.[1,6,7] This, of course, increases the number of parameters characterizing the free electron laser, but at the same time introduces greater complexity into the theory. The vector potential is now dependent on x and y and the perpendicular canonical momentum $\mathbf{P}_\perp$ is no longer a constant of motion; as a result, in general, no simple analytic solution for the electron trajectories can be found. Although so called "steady-state" helical trajectories with the same period as that of the wiggler and constant values of $|\mathbf{v}_\perp|$ and $|\mathbf{v}_\parallel|$ are allowed by the system, they cannot be obtained with arbitrary inlet conditions in the electron beam. Nevertheless, these are the trajectories usually used in the theory,[4,8] without studying the problem of how the steady-state situation can be achieved. An additional complication with the presence of an axial magnetic field is that, as will be shown in Sec. II of this paper, in general, there exist several possible steady-state trajectories for the same values of the axial field and wiggler parameters, and the question arises as to which of these states is accessible with given inlet conditions of the electron beam. Thus, in the presence of an axial guide field the initial conditions and the structure of the transition region at the entrance of the free electron laser may be of crucial importance in regard to the possible modes of operation of the device. These factors become even more important if the idea of recycling[9] is applied, and the electrons are forced to pass the transition region many times.

This paper presents a study of these important questions. In Sec. II, we derive the possible steady states in the homogeneous part of a free electron laser and study the stability of these states to perturbations of electron velocities. The transition region is included in the theory in Sec. III, where the possible ways of operating a free electron laser in different steady states are suggested and illustrated by numerical examples.

II. EQUATIONS OF MOTION AND STABILITY

Consider a cold relativistic electron beam moving in a magnetic field of the form

$$\mathbf{B} = \hat{B}(z)\mathbf{e}_z + \nabla \times \mathbf{A}, \tag{1}$$

where

$$\mathbf{A} = -\hat{A}(z)[\mathbf{e}_x \cos\phi(z) + \mathbf{e}_y \sin\phi(z)], \tag{2}$$

and

$$\phi = \int_0^z k_0(z')\,dz'. \tag{3}$$

For $\hat{A}$ and k_0 independent of z, the vector potential (2) describes the field on the axis of an infinite magnetic wiggler, where, as is well-known[10]

$$\hat{A} \propto I[\rho k_0 K_0(\rho k_0) + K_1(\rho k_0)], \tag{4}$$

where I is the current in the wiggler, ρ is its radius, $k_0 = 2\pi/\lambda_0$, λ_0 is the pitch of the winding of the wiggler, and $K_{0,1}$ are the modified Bessel functions of the second kind. By using the more general form (2) for the vector

 0031-9171/80/122376-07$00.90

potential, we have in mind primarily the possibility of slow variations of the wiggler parameters ρ and k_0 with z, and assume that in this case the magnitude $\hat{A}(z)$ in (2) can be approximated by expression (4), where ρ and k_0 correspond to the values of these parameters in the nonuniform wiggler at point z.

Although the magnetic field represented by the potential (2) does not satisfy $\nabla \times \mathbf{B} = 0$, it gives a good approximation of the exact curl-free field on an infinite wiggler at small distances r from its axis. Indeed, as was shown in Ref. 4, the relative deviation of the transverse component of the field from that described by (2) is of the order of $(k_0 r)^2$. Accordingly, if the beam radius l is such that $(k_0 l)^2 \ll 1$, the actual transverse field can be well represented by Eq. (2). The axial component of the field of a wiggler near the axis grows[4] as $k_0 r$; it can be neglected, however, in the presence of a strong axial guide field. We will also limit ourselves to low current beams so that the influence of the self-space charge on the beam can be neglected. We thus require that the transverse electrostatic field be much smaller than $v_\parallel B_\perp / c = v_\parallel k_0 \hat{A} / c$, or, assuming axial symmetry of the beam, $\omega_p^2 \gamma \ll 2ek_0 \hat{A} v_\parallel / mc$, where ω_p is the plasma frequency. If, for example, $r = 0.3$ cm, $B = 500$ G, and $v_\parallel \simeq c$, the maximum current density allowed by the model will be approximately 250 A/cm^2. The small signal gain in a free electron laser at these conditions, however, may be substantial,[11] so that the results of the present work could be important in current experiments.

We now consider the momentum equation for the electrons of the beam

$$\frac{d}{dt}(\gamma \mathbf{v}) = -\frac{e}{mc}\mathbf{v} \times \mathbf{B}, \tag{5}$$

where

$$\gamma = [1 - (v^2/c^2)]^{-1/2}. \tag{6}$$

Let

$$\begin{aligned} \mathbf{e}_1(z) &= -\mathbf{e}_x \sin\phi + \mathbf{e}_y \cos\phi, \\ \mathbf{e}_2(z) &= -\mathbf{e}_x \cos\phi - \mathbf{e}_y \sin\phi, \\ \mathbf{e}_3(z) &= \mathbf{e}_z. \end{aligned} \tag{7}$$

Then, the cononical model vector potential is

$$\mathbf{A} = \hat{A}(z)\mathbf{e}_2, \tag{8}$$

and

$$\mathbf{B} = \hat{B}(z)\mathbf{e}_3 - \frac{d\hat{A}}{dz}\mathbf{e}_1 - k_0 \hat{A}\mathbf{e}_2. \tag{9}$$

On expressing the velocity $\mathbf{v}$ in terms of the orthogonal vectors $\mathbf{e}_1$, $\mathbf{e}_2$, and $\mathbf{e}_3$ and using

$$\frac{d\mathbf{e}_1}{dt} = k_0 v_3 \mathbf{e}_2; \quad \frac{d\mathbf{e}_2}{dt} = -k_0 v_3 \mathbf{e}_1, \tag{10}$$

one can rewrite (5) as

$$\begin{aligned} \gamma \frac{dv_1}{dt} &= \gamma k_0 v_2 v_3 - \frac{e}{mc}(v_2 \hat{B} + k_0 v_3 \hat{A}), \\ \gamma \frac{dv_2}{dt} &= -\gamma k_0 v_1 v_3 + \frac{e}{mc}\left(v_1 \hat{B} + v_3 \frac{d\hat{A}}{dz}\right), \\ \gamma \frac{dv_3}{dt} &= \frac{e}{mc}\left(k_0 v_1 \hat{A} - v_2 \frac{d\hat{A}}{dz}\right). \end{aligned} \tag{11}$$

On using normalized velocities $u_i = v_i/c$ and "time" $\tau = ct$ and defining $\xi(z) = e\hat{A}/mc^2$ and $\Omega = e\hat{B}/mc^2$, one can write (11) in the form

$$\dot{u}_1 = u_2\left(k_0 u_3 - \frac{\Omega}{\gamma}\right) - \frac{k_0 \xi}{\gamma} u_3, \tag{12}$$

$$\dot{u}_2 = -u_1\left(k_0 u_3 - \frac{\Omega}{\gamma}\right) + \frac{1}{\gamma}\frac{d\xi}{dz} u_3, \tag{13}$$

$$\dot{u}_3 = \frac{k_0 \xi}{\gamma} u_1 - \frac{1}{\gamma}\frac{d\xi}{dz} u_2. \tag{14}$$

First consider the homogeneous case, where $\Omega = \Omega_0 = \text{const}$, $k_0 = \text{const}$, and $\xi = \xi_0 = \text{const}$. In this case, Eqs. (12)–(14) have a particular solution

$$u_{10} = 0, \quad u_{30} = \text{const},$$

and

$$u_{20} = \frac{k_0 \xi_0 u_{30}/\gamma}{k_0 u_{30} - \Omega/\gamma}, \tag{15}$$

which with the conservation of energy

$$1/\gamma^2 = 1 - u_{20}^2 - u_{30}^2 \tag{16}$$

defines the values of u_{20} and u_{30}. The question arises as to how this steady-state solution can be achieved. One can answer this question only by considering the transition region of the wiggler, where ξ and k_0 may depend on z. Here, one would expect that for initial conditions in the beam $u_1 = u_2 = 0$, when the vector potential ξ grows slowly enough with z, the velocities u_2 and u_3 would gradually approach their steady-state values u_{20} and u_{30}, and at the same time u_1 remains zero. It can be shown, however, that, in general, this cannot be the case. In fact, one gets from (13) that if $u_1(z) \equiv 0$,

$$\dot{u}_2 - \frac{1}{\gamma}\frac{d\xi}{dz} u_3 = u_3 \frac{d}{dz}\left(u_2 - \frac{\xi}{\gamma}\right) = 0, \tag{17}$$

and therefore $u_2 = \xi/\gamma$, which, on using (12), requires that $\Omega(z) \equiv 0$. Thus, in the presence of an axial magnetic field and for the initial conditions on u considered here, u_1 cannot remain zero in the transition region. The maximum that can be expected is that the component u_1 in the transition region remains small in comparison with u_2 and u_3. When this is the case, and, in addition, u_1 remains small as the beam propagates in the homogeneous part of the wiggler we define the beam to be *stable* and now proceed to the study of this special kind of stability.

First, consider the homogeneous region of the device and in this region let

$$u_1(\tau) = w_1(\tau), \quad u_2(\tau) = u_{20} + w_2(\tau), \quad u_3(\tau) = u_{30} + w_3(\tau), \tag{18}$$

where u_{20} and u_{30} are given by (15) and (16), and $w_i(\tau)$ are small perturbations to the steady-state solution. Then, on linearizing Eqs. (12)–(14) one gets

$$\dot{w}_1 = aw_2 + bw_3, \tag{19}$$

$$\dot{w}_2 = -aw_1, \tag{20}$$

$$\dot{w}_3 = cw_1, \tag{21}$$

where

$$a = k_0 u_{30} - \frac{\Omega}{\gamma} = \frac{k_0 \xi_0}{\gamma} \frac{u_{30}}{u_{20}}, \tag{22}$$

$$b = k_0 u_{20} - \frac{k_0 \xi_0}{\gamma} = \frac{\Omega}{\gamma} \frac{u_{20}}{u_{30}}, \tag{23}$$

$$c = k_0 \xi_0 / \gamma . \tag{24}$$

Equation (19) then gives

$$\ddot{w}_1 = a\dot{w}_2 + b\dot{w}_3 = -(a^2 - bc) w_1 . \tag{25}$$

Thus, the necessary condition for the stability of the electron beam is

$$a^2 - bc > 0 , \tag{26}$$

or

$$\frac{\Omega}{k_0 \xi_0} \left(\frac{u_{20}}{u_{30}} \right)^3 < 1 . \tag{27}$$

Further study of the stability problem must involve a knowledge of u_{20} and u_{30}. Let us combine Eqs. (15) and (16); there results

$$1 - u_{30}^2 - \left(\frac{\xi}{\gamma} \right)^2 \frac{u_{30}^2}{(u_{30} - \Omega/\gamma k_0)^2} = \frac{1}{\gamma^2} . \tag{28}$$

This equation can be rewritten in the form

$$F = F_1 - F_2 = 0 , \tag{29}$$

where

$$F_1 = \frac{1 - 1/\gamma^2}{u_{30}^2} , \tag{30}$$

and

$$F_2 = 1 + \frac{(\xi_0/\gamma)^2}{(u_{30} - \Omega/k_0\gamma)^2} . \tag{31}$$

Assuming $(\xi_0/\gamma)^2 < 1 - 1/\gamma^2$ for γ large enough, the functions F_1 and F_2 have the general form shown in Fig. 1 for various values of Ω. It can be seen from Fig. 1(a) that for $\Omega = 0$, there are two solutions for u_{30}, corresponding to different directions of propagation of the

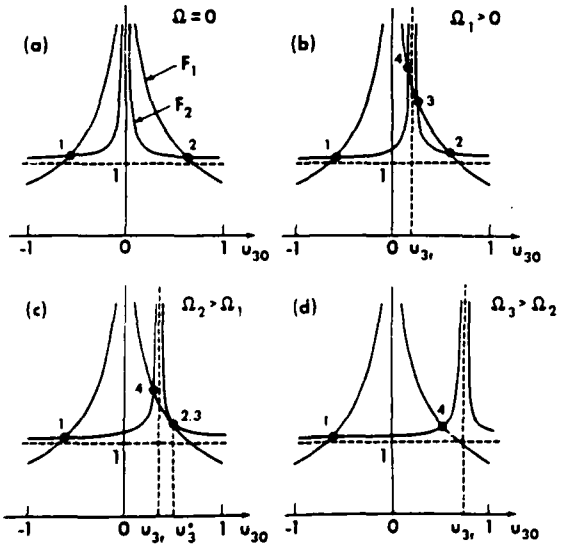

FIG. 1. Schematic of the functions F_1 and F_2, defining various possible steady-state solutions for u_{30}.

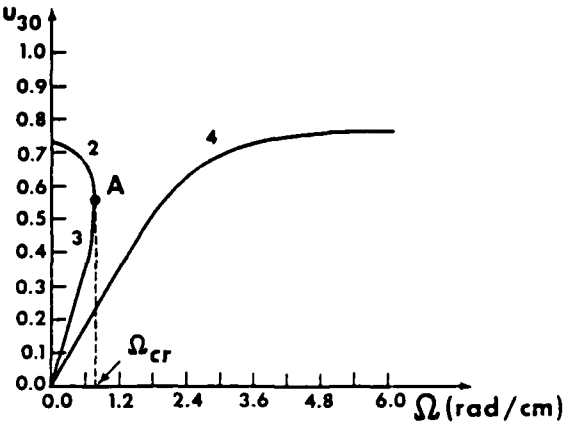

FIG. 2. The real positive branches of u_{30} vs the cyclotron frequency Ω, characterizing the guide magnetic field.

electron beam. In the presence of a weak axial magnetic field, there exist two additional solutions for u_{30} adjacent to the resonance velocity $u_{3r} = \Omega/k_0\gamma$, as shown in Fig. 1(b). If one continues to increase Ω, a situation is reached, where again there remain only two real solutions for u_{30} [Figs. 1(c), (d)]. The diagram, where all possible real positive branches of u_{30} are presented as a function of Ω, is given in Fig. 2 for a sample case in which $\gamma = 1.587$, $k_0 = 1.5708\ \mathrm{cm}^{-1}$, and $\xi_0 = 0.3873$.

Let us now find the frequency Ω_{cr} at which the roots 2 and 3 on Fig. 2 become complex. This transition corresponds to the point A on the figure. One can find Ω_{cr} by observing that the function F in Eq. (29) has only one bounded maximum at the point u_3^*, such that $F'(u_3^*) = 0$, or

$$u_3^* = \frac{\Omega}{\alpha k_0 \gamma} , \tag{32}$$

where

$$\alpha = 1 - \left(\frac{(\xi_0/\gamma)^2}{1 - 1/\gamma^2} \right)^{1/3} . \tag{33}$$

It is now clear that when F has four real roots, they are contained in the following intervals: $[-1, 0]$, $[0, u_{3r}]$, $[u_{3r}, u_3^*]$, $[u_3^*, +1]$. On the ends of these intervals the function F changes its sign, which makes it easy to find the four roots numerically. It is also clear that the roots in the last two intervals become complex, when $F(u_3^*) = 0$. Simple algebra then leads to the following expression for Ω_{cr}:

$$\Omega_{cr} = k_0 \gamma \alpha^{3/2} \left(1 - \frac{1}{\gamma^2} \right)^{1/2} . \tag{34}$$

Considering our sample case shown in Fig. 2, Eq. (34) gives the value $\Omega_{cr} = 0.763$ rad/cm.

We now return to the question of stability. It is clear that inequality (27) (which is the necessary condition for the stability) is satisfied for branch 4 in Fig. 2, since, according to (15), u_{20} is negative on this branch. Simple analysis also shows that branch 2 is stable, since the left-hand side of (27) on this branch reaches its maximum value of 1 only at $\Omega = \Omega_{cr}$; branch 3, in contrast, is always unstable.

III. TRANSITION REGION

The inequality (27) is a necessary condition for stability of the electron beam in the homogeneous part of free electron laser. This condition becomes sufficient if the electron beam enters the homogeneous region with small enough component u_1 in its velocity. We now proceed to the study of the transition region, where as will be shown, special experimental steps must be taken in order to get a stable electron beam, corresponding to various branches on the diagram on Fig. 2. Let us assume that the vector potential ξ in the transition region is a slowly growing function of z. Experimentally, this would be the case, for example, if one gradually decreases the radius ρ of the wiggler, or increases the pitch length $\lambda_0 = 2\pi/k_0$ at the end of the device as can be seen from Eq. (4). Following the ideas used in the previous section, one can find approximate solutions of (12)–(14) by using expansions (18), where u_{20} and u_{30} are now functions of z and correspond to the components of the velocity in the homogeneous case with parameters such as those at the point z in the transition region. Then, similar to (19)–(21) one has

$$\dot{w}_1 = aw_2 + bw_3 , \tag{35}$$

$$\dot{w}_2 = -aw_1 + fu_{30} , \tag{36}$$

$$\dot{w}_3 = cw_1 - fu_{20} , \tag{37}$$

where a, b, and c are given by (22)–(24) and

$$f = \frac{1}{\gamma}\frac{d\xi}{dz} . \tag{38}$$

Taking the time derivative of Eq. (35) and assuming that the coefficients a and b are slowly varying functions of z, one gets the following equation

$$\ddot{w}_1 = a\dot{w}_2 + b\dot{w}_3 + \dot{a}w_2 + \dot{b}w_3 \simeq a\dot{w}_2 + b\dot{w}_3$$
$$= -(a^2 - bc)w_1 + f(au_{30} - bu_{20}) , \tag{39}$$

or, on using (22)–(24)

$$\ddot{w}_1 = -\mu^2 w_1 + g , \tag{40}$$

where

$$\mu^2 = a^2 - bc , \tag{41}$$

and

$$g = \mu^2 \frac{u_{20}\gamma}{k_0 \xi} f . \tag{42}$$

Assuming that μ is a slowly varying function of τ one can approximate the solution of the homogeneous equation

$$\ddot{w}_1 = -\mu^2 w_1 , \tag{43}$$

by the WKB solution

$$w_1(\tau) = \mu^{-1/2}[C_1 \cos\psi(\tau) + C_2 \sin\psi(\tau)] , \tag{44}$$

where

$$\psi = \int_0^\tau \mu(\tau')\, d\tau' . \tag{45}$$

Then, it can be easily shown, using the method of variation of constants in (44), that the solution of the inhomogeneous equation (40), with the initial conditions $w_1|_0 = \dot{w}_1|_0 = 0$, can be expressed as

$$w_1(\tau) = \frac{1}{\mu^{1/2}(\tau)} \int_0^\tau \frac{g(\tau')}{\mu^{1/2}(\tau')} \sin[\psi(\tau) - \psi(\tau')]\, d\tau' . \tag{46}$$

Thus, if the vector potential ξ grows slowly in the transition region (the function $f = 1/\gamma\, d\xi/dz$ is small enough), one expects the electron beam to enter the homogeneous part of the wiggler with a small magnitude of w_1, which is sufficient for the stability of the beam in this region if the inequality (27) is satisfied.

In such an adiabatic case, one can also find the trajectories of the electrons passing the transition region. Expressing the radius vector $\mathbf{r}$ of the electrons in the beam in terms of the unit vectors $\mathbf{e}_1$, $\mathbf{e}_2$, and $\mathbf{e}_3$ [see Eq. (7)], one has

$$\mathbf{r} = r_1\mathbf{e}_1 + r_2\mathbf{e}_2 + z\mathbf{e}_3 , \tag{47}$$

which on differentiation with respect to τ gives

$$\dot{\mathbf{r}} = (\dot{r}_1 - k_0 u_3 r_2)\mathbf{e}_1 + (\dot{r}_2 + k_0 u_3 r_1)\mathbf{e}_2 + \dot{z}\mathbf{e}_3 , \tag{48}$$

and therefore the trajectories are described by

$$\dot{r}_1 = u_1 + k_0 u_3 r_2 , \quad \dot{r}_2 = u_2 - k_0 u_3 r_1 . \tag{49}$$

This system of equations can be solved in the following way: Let

$$R = r_1 + ir_2 , \quad U = u_1 + iu_2 . \tag{50}$$

Then, on multiplying the second equation in (49) by i and adding it to the first equation, one gets

$$\dot{R} = U - ik_0 u_3 R . \tag{51}$$

If one splits R into two parts

$$R = R_0 + R_1 , \tag{52}$$

where

$$iR_0 = U/k_0 u_3 , \tag{53}$$

and R_1 is assumed to be small, then on linearization in Eq. (51),

$$\dot{R}_1 = -\dot{R}_0 - ik_0 u_3 R_1 . \tag{54}$$

The solution of this equation for R_1 is given by

$$R_1 = -\int_0^\tau \dot{R}_0(\tau') \exp(-i\{\phi[z(\tau)] - \phi[z(\tau')]\})\, d\tau' , \tag{55}$$

where ϕ is defined by (3). Thus, if the velocities u_1, u_2, and u_3 are slowly varying functions in the transition region, R_1 remains small along the trajectories and $R \simeq R_0$, or

$$r_1(z) \simeq \mathrm{Re}(R_0) \simeq \frac{u_{20}(z)}{k_0(z)u_{30}(z)} , \tag{56}$$

$$r_2(z) \simeq \mathrm{Im}(R_0) \simeq -\frac{u_{10}(z)}{k_0(z)u_{30}(z)} \ll r_1(z) , \tag{57}$$

and therefore the electrons in this case are moving on helical orbits with adiabatically changing radius r_1, and the pitch period as that of the wiggler.

Thus, we have shown that, in principle, one can obtain a stable electron beam in a free electron laser if the variations of the parameters of the wiggler in the transition region are slow enough. This conclusion,

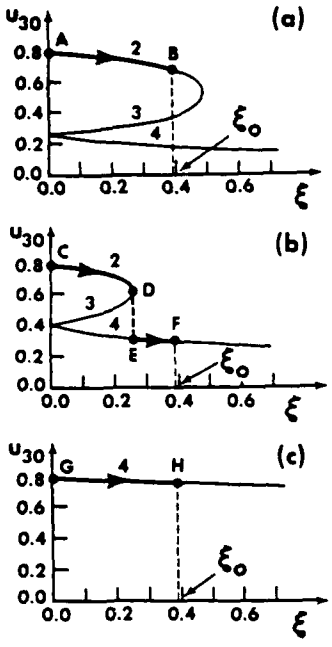

FIG. 3. The real positive branches of u_{30} vs ξ. (a) $\Omega = 0.6$ rad/cm; (b) $\Omega = 1.0$ rad/cm; (c) $\Omega = 4.0$ rad/cm.

however, is based on the approximate solution (46) for w_1 and one has to check whether all the assumptions, used in the derivation of this solution, are correct. One of these assumptions was the slowness of variation of the coefficients a and b in (35) as the beam propagates through the transition region. Let us show now that, in general, this is not guaranteed even if ξ varies slowly. The reason is that the real solutions for u_{20} and u_{30}, which are used in the definitions of a and b, do not always behave continuously. We demonstrate such a possibility in Fig. 3. In this figure, one can see the diagrams of the possible real positive solutions for u_{30}, obtained in a fashion similar to the diagram in Fig. 2, but for constant values of Ω and varying ξ. Our sample case parameters $\gamma = 1.587$ and $k_0 = 1.5708$ were again used in these graphs. As mentioned previously, the variation of ξ with constant value of k_0 can be experimentally obtained by varying the radius of the wiggler winding in the transition region, holding the pitch length $\lambda_0 = 2\pi/k_0$, constant. In Figs. 3(a,b), we show two cases with the values of Ω higher and lower than the critical value Ω_{cr} in the homogeneous region [Ω_{cr} is defined by Eq. (34), and in our sample case is equal to 0.763 rad/cm]. For $\Omega < \Omega_{cr}$, as ξ increases in the transition region, one follows the path AB in Fig. 3(a) and passes continuously to the homogeneous region corresponding to the point B on the diagram (at this point $\xi = \xi_0$). The beam is stable in this case. In contrast, if Ω is larger than Ω_{cr}, one arrives in the transition region at the point D [see Fig. 3(b)], where the branches 2 and 3 of u_{30} become complex and the homogeneous region can be only reached on the diagram by the discontinuous path DEF. The jump DE in u_{30} leads to the fast variation on the right-hand side of Eq. (12), which cannot remain small anymore, and u_1 grows in amplitude, leading to the instability of the beam. For sufficiently large values of Ω, one can again return to the stable regime. In fact, if $u_{3r} = \Omega/\gamma k_0 > 1$,

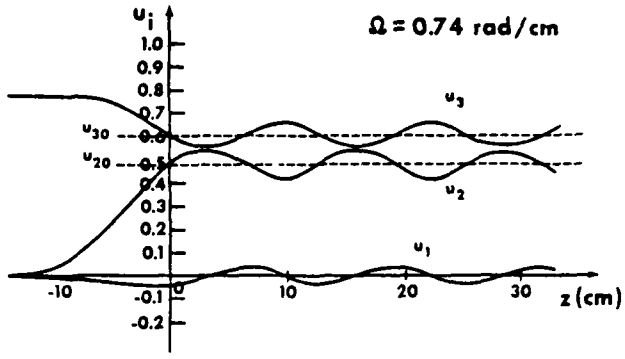

FIG. 4. The z dependence of various components of the electron velocities for $\Omega = 0.74$ rad/cm.

the only possible real branch of u_{30} is branch 4 (see Fig. 2). This situation is illustrated in Fig. 3(c). The beam follows a continuous path GH in the transition region in this case and remains stable.

In addition to these qualitative considerations, we illustrate the creation of the instability in the beam in Figs. 4 and 5, where the numerical solutions of Eqs. (12)–(14) for u_i are presented for our sample case for two values of $\Omega = 0.74$ and 0.77 rad/cm (recall that $\Omega_{cr} = 0.763$ rad/cm). We assumed in these calculations the following z dependence of the radius ρ of the wiggler winding in the transition region:

$$\rho = \begin{cases} \rho_0, & z \geq 0; \\ \rho_0 + (z/z_0)^2, & z < 0, \end{cases} \tag{58}$$

where $\rho_0 = 2.5$ cm and $z_0 = 8$ cm. The sudden transition to the unstable behavior when one goes from Fig. 4 to Fig. 5, where all the u_i's change rapidly (u_3 even becomes negative on the parts of the trajectory) is obvious.

Thus, in conclusion, if the vector potential ξ varies

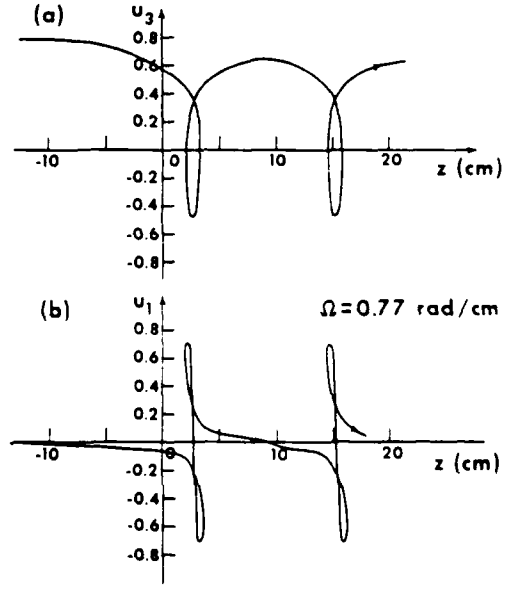

FIG. 5. The z dependence of u_1 and u_3 for $\Omega = 0.77$ rad/cm.

slowly in the transition region, one can get a stable electron beam for $\Omega < \Omega_{cr}$, and as the parameters of the wiggler vary adiabatically, the beam follows branch 2 of the possible solutions for u_{3_0} on Fig. 2. One can also have a stable situation for large axial magnetic fields, when branch 4 remains the only possible one for operation. One has to remember, however, that the necessary condition for the last possibility is that in the transition region $u_{3_r} = \Omega/k_0\gamma > 1$. This condition can easily be satisfied when the growth of ξ in the transition region is due to the variation of the radius ρ of the wiggler, when $k_0 = \text{const}$. If in contrast, $\rho = \text{const}$ and k_0 is increasing as one approaches the end of the wiggler, larger values of the axial magnetic field are required in order to operate the device on branch 4.

Let us finally consider the question of whether it is possible with the initial conditions on the beam assumed here (namely, $u_1|_0 = u_2|_0 = 0$) to get a stable electron beam at a larger region of branch 4, especially for $u_{3_r} \lesssim 1$. As mentioned before, the necessary condition (27) for stability is always satisfied on this branch, which makes it more attractive. The perpendicular component of the velocity on branch 4 can also become very large, which is again very important for possible electromagnetic wave amplification in the z direction.

The experimental scheme, which allows one to operate a free electron laser on branch 4 is shown in Fig. 6. We are exploiting the stability of the beam for large values of Ω [as demonstrated in Fig. 3(c)] and are applying a strong axial magnetic field in the transition region of the wiggler. Then, after passing this region the electrons will enter the homogeneous part of the wiggler, being on the upper part of branch 4 in Fig. 2. Now in the homogeneous region, where $\xi = \xi_0 = \text{const}$, one can gradually reduce the axial magnetic field. The beam will then follow the continuous branch 4 and one can easily reach region $\Omega \simeq \Omega_{cr}$, which was unstable with the constant axial magnetic field. We demonstrate this possibility in Fig. 7, where the solutions of Eqs. (12)–(14) are shown for exactly the same final Ω and ξ_0 as in the unstable case in Fig. 5. The same variation (58) for ρ was used in the computations. The cyclotron frequency was assumed to have the form

$$\Omega = \begin{cases} \Omega_1, & z \leq 2L, \\ (\Omega_1 - \Omega_2)e^{-(z-2L)^2/L^2} + \Omega_2, & z > 2L, \end{cases} \tag{59}$$

where $\Omega_1 = 4$ rad/cm, $\Omega_2 = 0.77$ rad/cm, and $L = 4$ cm. It can be seen from Fig. 7 that the beam remains stable and corresponds to branch 4 with negative and larger values of u_{2_0} than in Fig. 4, which corresponds to branch 2.

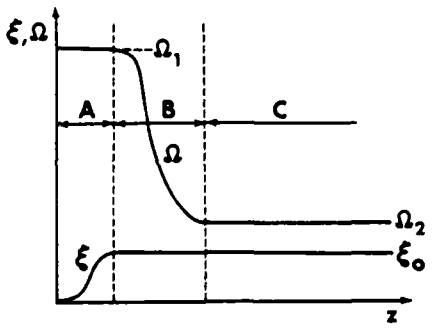

FIG. 6. Possible configuration of the pump and guide fields for operating on branch 4 of the steady-state regimes. A–transition region for ξ; B–transition region for Ω; C–homogenous part of the device.

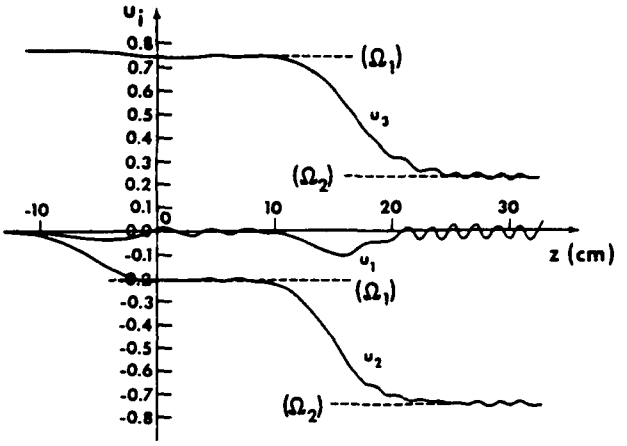

FIG. 7. The z dependence of the electron velocities in operating on branch 4 with varying guide magnetic field. Ω = 4 rad/cm, Ω = 0.77 rad/cm.

IV. CONCLUSIONS

(i) In operating a free electron laser with an axial magnetic field, different steady-state regimes of the helical motion of the electrons in the homogeneous part of the wiggler must be considered.

(ii) The necessary condition for the stability of these steady-state regimes is given by the inequality (27).

(iii) The transition region of a free electron laser plays an important role in determining the sufficient conditions for stability and in achieving the different modes of operation of a free electron laser for a given set of parameters of the homogeneous part of the device.

(iv) The following two models have been analyzed for operating a free electron laser in different steady-state regimes:

(a) The first is characterized by a constant axial magnetic field and gradual increase in the vector potential in the transition region. The stability of this scheme is limited by a critical value of the axial field given by Eq. (34). The value of the perpendicular component of the velocity is also limited in this steady-state regime.

(b) The second setup uses a strong axial magnetic field in the transition region. The field is then adiabatically decreased in the homogeneous part of the wiggler. This regime is always stable and can operate with any value of the axial magnetic field in the homogeneous region. The only limitation is imposed by the increasing radius of the helical trajectories of the electrons in the beam

as the perpendicular component of the velocities grows with a decrease in the axial guide field.

ACKNOWLEDGMENTS

The author wishes to express his appreciation to Professors I. B. Bernstein and J. L. Hirshfield for many useful discussions.

This work was supported in part by the Office of Naval Research and the Department of Energy.

[1]L. R. Elias, W. M. Fairbank, J. M. J. Madey, H. A. Schwettman, and T. I. Smith, Phys. Rev. Lett. 36, 717 (1976).
[2]H. Motz, J. Appl. Phys. 22, 527 (1951).
[3]I. B. Bernstein and J. L. Hirshfield, Phys. Rev. Lett. 40, 761 (1978).
[4]J. P. Blewett and R. Chasman, J. Appl. Phys. 48, 2692 (1977).
[5]Fo a review see P. Sprangle, R. A. Smith, and V. L. Granatstein, in *Infrared and Millimeter Waves*, edited by K. Button (Academic, New York, 1979), Chap. 7, p. 279.
[6]T. C. Marshall, S. Talmadge, and P. Efthimion, Appl. Phys. Lett. 31, 320 (1977).
[7]R. M. Gilgenbach, T. C. Marshall, and S. P. Schlesinger, Phys. Fluids 22, 1219 (1979).
[8]T. Kwan and J. M. Dawson, Phys. Fluids 22, 1089 (1979).
[9]L. R. Elias, Phys. Rev. Lett. 42, 977 (1979).
[10]W. R. Smythe, *Static and Dynamic Electricity* (McGraw-Hill, New York, 1950), p. 277.
[11]W. B. Colson, in *Physics of Quantum Electronics* (Addison-Wesley, New York, 1977), Vol. 5, p. 152.

Theory of the free-electron laser in combined helical pump and axial guide fields

Ira B. Bernstein and Lazar Friedland
Department of Engineering and Applied Science, Yale University, New Haven, Connecticut 06520
(Received 7 July 1980)

The linearized theory of a free-electron-laser amplifier consisting of a relativistic electron beam transported along the axis of a helical wiggler in the presence of an axial guide field is solved exactly. With suitable re-identification of parameters, the theory also applies to the case where the wiggler is replaced by a circularly polarized subluminous radio-frequency pump. The dispersion relation is derived and numerical examples of solutions are presented. These indicate (a) that the use of an axial field permits operation of a laser of given high frequency and undulatory transverse velocity of the unperturbed electron beam at lower values of the pump field, (b) that the gain can be enhanced by approaching the condition of resonance between the effective frequency of the pump and the cyclotron frequency, and (c) that the breadth in frequency of the region corresponding to spatially exponentially growing operation can be much extended.

I. INTRODUCTION

The theory of a free-electron laser (FEL), consisting of a relativistic electron beam transported along the axis of a helical pump magnetic field, has been given by Bernstein and Hirshfield.[1] Their analysis was valid for arbitrary pump strength but weak rf fields, since it involved linearization in the amplitudes of the high-frequency quantities. Here we present the extension of that work to the case where, in addition, there is an axial magnetic field, conventionally present for beam collimation. It is also shown that with a suitable reinterpretation of parameters, the same theory applies when the magnetostatic pump is replaced by a circularly polarized subluminous rf pump. The axial field is shown to yield the additional benefits of permitting the use of weaker pumps, providing enhanced gain and yielding broader domains of spacial instability. This is discussed in detail in Sec. VI.

The work proceeds as follows. The general mathematical description is developed in Sec. II where the continuity and momentum equations describing the relativistic beam, and those governing the electromagnetic fields are presented. Section III describes the properties of a helical pump magnetostatic field, and Sec. IV those of a circularly polarized subluminous rf pump. The linearized equations governing the high-frequency fields are derived in Sec. V. Section VI is devoted to a brief discussion of the relation of this work to its predecessors, to a description of the numerical examples worked out, and conclusions concerning the effects of the axial field.

II. GENERAL MATHEMATICAL DESCRIPTION

Consider a cold relativistic electron beam described by the continuity equation

$$\frac{\partial N}{\partial t}+\nabla\cdot(N\vec{v})=0 \tag{1}$$

and the momentum equation

$$\left(\frac{\partial}{\partial t}+\vec{v}\cdot\nabla\right)(m\gamma\vec{v})=-e\left(\vec{E}+\vec{v}\times\frac{\vec{B}}{c}\right), \tag{2}$$

where m is the rest mass of the electron, and

$$\gamma=(1-v^2/c^2)^{-1/2} \tag{3}$$

If one forms the scalar product of (2) with $\gamma\vec{v}$ and uses (3) to express v in terms of γ, there results the energy equation

$$\left(\frac{\partial}{\partial t}+\vec{v}\cdot\nabla\right)mc^2\gamma=-e\vec{E}\cdot\vec{v}. \tag{4}$$

Let $\hat{B}$ be a constant. It is convenient to introduce the electromagnetic potential $\vec{A}$ and Φ via

$$\vec{B}=\hat{B}\vec{e}_z+\nabla\times\vec{A}, \tag{5}$$

$$\vec{E}=-\nabla\Phi-\frac{\partial}{\partial t}\left(\frac{\vec{A}}{c}\right). \tag{6}$$

Then with $\Omega=e\hat{B}/mc$ one can write (2) in the form

$$\begin{aligned}&\left(\frac{\partial}{\partial t}+\vec{v}\cdot\vec{\nabla}\right)(m\gamma\vec{v})\\&=-\left(\frac{e}{c}\right)\left(-c\nabla\Phi-\frac{\partial\vec{A}}{\partial t}+\vec{v}\times(\nabla\times\vec{A})+\hat{B}\vec{v}\times\vec{e}_z\right)\\&=m\Omega\vec{e}_z\times\vec{v}+\left(\frac{e}{c}\right)\left(c\nabla\Phi+\frac{\partial\vec{A}}{\partial t}+\vec{v}\cdot\nabla\vec{A}-(\nabla\vec{A})\cdot\vec{v}\right)\end{aligned} \tag{7}$$

or on rearranging terms

$$\begin{aligned}&\left(\frac{\partial}{\partial t}+\vec{v}\cdot\vec{\nabla}\right)\left(\gamma\vec{v}-\frac{e\vec{A}}{mc}\right)\\&=\Omega\vec{e}_z\times\vec{v}+\left(\frac{e}{mc}\right)[c\nabla\Phi-(\nabla\vec{A})\cdot\vec{v}].\end{aligned} \tag{8}$$

It follows from the Maxwell equations

$$c\nabla\times\vec{B}=4\pi\vec{J}+\frac{\partial\vec{E}}{\partial t}, \tag{9}$$

$$\nabla\cdot\vec{E}=4\pi\Sigma, \tag{10}$$

on employing (5) and (6), that

$$\nabla^2\vec{A}-c^{-2}\frac{\partial^2\vec{A}}{\partial t^2}+\left(\frac{4\pi}{c}\right)\vec{J}=\nabla\left(c^{-1}\frac{\partial\Phi}{\partial t}+\vec{\nabla}\cdot\vec{A}\right), \tag{11}$$

$$\nabla^2\Phi+4\pi\Sigma=-c^{-1}\nabla\cdot\frac{\partial\vec{A}}{\partial t}. \tag{12}$$

Thus if we adopt the canonical model of FEL theory, viz.

$$\vec{A}=A_x(z,t)\vec{e}_x+A_y(z,t)\vec{e}_y, \tag{13}$$

$$\Phi=\Phi(z,t) \tag{14}$$

(note that the vector potential is written in the Coulomb gauge) and assume that the only charged particles present are electrons, whence $\Sigma=-Ne$ and $\vec{J}=-Ne\vec{v}$, then (11) and (12) yield

$$\frac{\partial^2\vec{A}}{\partial z^2}-c^{-2}\frac{\partial^2\vec{A}}{\partial t^2}=\left(\frac{4\pi Ne}{c}\right)(\vec{v}-\vec{e}_z\vec{e}_z\cdot\vec{v}), \tag{15}$$

$$\frac{\partial^2\Phi}{\partial z^2}=4\pi Ne. \tag{16}$$

III. MAGNETOSTATIC PUMP

Consider the case of a free-electron laser in which the pump magnetostatic field is generated by helical windings and the self-fields of the electron beam are negligible. Then in cylindrical coordinates ρ,θ,z the vacuum magnetic scalar potential χ will be helically invariant, viz.

$$\chi=\chi(\rho,\theta-k_0z), \tag{17}$$

where $2\pi/k_0$ is the pitch, and will satisfy Laplace's equation

$$\nabla^2\chi=\frac{1}{\rho}\frac{\partial}{\partial\rho}\left(\rho\frac{\partial\chi}{\partial\rho}\right)+\left(k_0^2+\frac{1}{\rho^2}\right)\frac{\partial^2\chi}{\partial\vartheta^2}=0. \tag{18}$$

The general solution of (18), regular at $\rho=0$, on separation of variables is readily shown to be

$$\chi=-\hat{B}z+\sum_{m=1}^{\infty}\chi_m I_m(mk_0\rho)\cos[m(\theta-k_0z)+\lambda_m], \tag{19}$$

where the χ_m and λ_m are constants determined by the details of the helical windings. Recall that the Bessel function

$$I_m(\zeta)=\sum_{s=0}^{\infty}\frac{(\frac{1}{2}\zeta)^{m+2s}}{s!\,(m+s)!}. \tag{20}$$

Thus if a is the radius of the windings and $\rho\ll 2\pi/k_0$, the potential is well approximated by the term with $m=1$ alone, with I_1 approximated by the leading term in the series. The resulting expression for the associated magnetic field is, on choosing the coordinate system so that $\lambda_1=0$ and $\frac{1}{2}k_0\chi_1=-B_0$,

$$\vec{B}=-\nabla\chi\approx\hat{B}\vec{e}_z+B_0(\vec{e}_x\cos k_0z+\vec{e}_y\sin k_0z). \tag{21}$$

The nonconstant part of (21) can be written as the curl of the vector potential

$$\vec{A}=-(B_0/k_0)(\vec{e}_x\cos k_0z+\vec{e}_y\sin k_0z). \tag{22}$$

Expression (22), valid only near the axis, is the form conventionally taken for the magnetostatic pump field. A corresponding solution for the velocity and density can be obtained from (1) and (8) by introducing the basis vectors

$$\vec{e}_1=-\vec{e}_x\sin k_0z+\vec{e}_y\cos k_0z, \tag{23}$$

$$\vec{e}_2=-\vec{e}_x\cos k_0z-\vec{e}_y\sin k_0z, \tag{24}$$

$$\vec{e}_3=\vec{e}_z, \tag{25}$$

when on writing

$$A=A_1\vec{e}_1+A_2\vec{e}_2+A_3\vec{e}_3 \tag{26}$$

it follows that

$$\frac{\partial\vec{A}}{\partial z}=\left(\frac{\partial A_1}{\partial z}-k_0A_2\right)\vec{e}_1+\left(\frac{\partial A_2}{\partial z}+k_0A_1\right)\vec{e}_2+\frac{\partial A_3}{\partial z}\vec{e}_3. \tag{27}$$

Thus (1) and (8) imply

$$\left(\frac{\partial}{\partial t}+\frac{v_3\partial}{\partial z}\right)N=-\frac{N\partial v_3}{\partial z}, \tag{28}$$

$$\left(\frac{\partial}{\partial t}+\frac{v_3\partial}{\partial z}\right)\left(\gamma v-\frac{eA_1}{mc}\right)-k_0v_3\left(\gamma v_2-\frac{eA_2}{mc}\right)=-\Omega v_2, \tag{29}$$

$$\left(\frac{\partial}{\partial t}+\frac{v_3\partial}{\partial z}\right)\left(\gamma v_2-\frac{eA_2}{mc}\right)+k_0v_3\left(\gamma v_1-\frac{eA_1}{mc}\right)=\Omega v_1, \tag{30}$$

$$\left(\frac{\partial}{\partial t}+\frac{v_3\partial}{\partial z}\right)(\gamma v_3)=\left(\frac{e}{mc}\right)\left(\frac{c\partial\Phi}{\partial z}-v_1\frac{\partial A_1}{\partial z}-v_2\frac{\partial A_2}{\partial z}-k_0v_2A_1+k_0v_1A_2\right). \tag{31}$$

Now on combining (22) and (25) one can write

$$\vec{A}_0=(mc^2/e)\xi_0\vec{e}_2, \tag{32}$$

where ξ_0 is a dimensionless constant. It is then readily seen that if also $\Phi_0=0$, corresponding to $E_0=-\nabla\Phi_0=0$, then a solution is given by

$$\vec{v}_0=u\vec{e}_3+w\vec{e}_2, \tag{33}$$

$$N_0=\text{const}, \tag{34}$$

where $u=\text{const}$ and $w=\text{const}$, satisfy (27)–(30) provided that consequent to (29)

$$w=k_0cu\xi_0(k_0u\gamma_0-\Omega)^{-1}: \tag{35}$$

where

$$\gamma_0 = [1 - (u^2 + w^2)/c^2]^{-1/2} \tag{36}$$

This solution and its experimental accessibility has been analyzed in detail by Friedland.[2]

IV. RADIO-FREQUENCY PUMP

The solution given by (32), (33), and (34) with $\vec{E}_0 = 0$ can also be adapted to describe the case of a free-electron laser with an electromagnetic pump which in the laboratory frame has a phase velocity less than the speed of light. One then views the solution as given in the frame where the pump wave is at rest. Equation (15) then requires, on using (32) and (33), that

$$-k_0^2 c^2 \xi_0 = \omega_p^2 w/c\,, \tag{37}$$

which on using (35) can be written

$$-k_0 c = \omega_p^2 \mu (k_0 \mu \gamma_0 - \Omega)^{-1}\,, \tag{38}$$

where the plasma frequency, defined using the rest mass, is

$$\omega_p = (4\pi N_0 e^2/m)^{1/2}\,. \tag{39}$$

Let v_0 be the speed of the laboratory frame as seen from the wave frame. Distinguish quantities in the laboratory frame by a prime. Then on Lorentz transformation $z' = \hat{\gamma}(z - v_0 t)$, $t' = \hat{\gamma}(t - v_0 z/c^2)$, and

$$\omega' = -k_0 v_0 \hat{\gamma}\,, \tag{40}$$

$$k_0' = k_0 \hat{\gamma}\,, \tag{41}$$

where

$$\hat{\gamma} = (1 - v_0^2/c^2)^{-1/2}\,. \tag{42}$$

Clearly

$$v_0 = -\omega'/k_0'\,, \tag{43}$$

is the negative of the phase velocity of the wave. Moreover,

$$\vec{B}_0' = \hat{B}\vec{e}_3 + B_0'[\vec{e}_x \cos(k_0' z' - \omega' t') + \vec{e}_y \sin(k_0' z' - \omega' t')]\,, \tag{44}$$

where

$$B_0' = \hat{\gamma} B_0 \tag{45}$$

and

$$\vec{E}_0' = -(\omega'/k_0' c)\vec{e}_3 \times \vec{B}_0'\,. \tag{46}$$

Evidently the wave is transverse and circularly polarized. The associated potentials are

$$\Phi_0' = 0\,, \tag{47}$$

$$\vec{A}_0' = A_0'[\vec{e}_x \cos(k_0' z' - \omega' t') + \vec{e}_y \sin(k_0' z' - \omega' t')]\,, \tag{48}$$

where

$$A_0' = -\frac{B_0'}{k_0'} = -\frac{B_0}{k_0} = \frac{mc^2}{e}\xi_0\,. \tag{49}$$

Clearly A_0' is a Lorentz invariant. Also

$$\gamma' = \gamma_0 \hat{\gamma}(1 - v_0 u/c^2)\,, \tag{50}$$

$$N' = N\hat{\gamma}(1 - v_0 u/c^2)\,, \tag{51}$$

$$u' = \frac{u - v_0}{1 - v_0 u/c^2}\,, \tag{52}$$

$$w' = \frac{w/\hat{\gamma}}{1 - v_0 u/c^2}\,. \tag{53}$$

The inverse transformations to (50)–(53) can be gotten by interchanging primed and unprimed variables and changing the sign of v_0.

The counterpart of (35) is now

$$w' = c\xi_0(k_0' u' - c_0')[\gamma_0'(k_0' u - \omega') - \Omega]^{-1}\,. \tag{54}$$

Equation (38) is carried into

$$(\omega'^2 - k_0'^2 c^2) = \omega_p'^2 (k_0' u' - \omega')[\gamma_0'(k_0' u' - \omega') - \Omega]^{-1}\,. \tag{55}$$

Equation (55) can be viewed as the dispersion relation for the pump electromagnetic field, but it is to be noted that the steady-state theory is not restricted to weak pump fields and a linearized theory.

V. STABILITY ANALYSIS

Let us work in the laboratory frame for the case of the magnetostatic pump and in the wave frame for the case of the radio-frequency pump. The stability analysis is then common. Let

$$\vec{A} = \vec{A}_0 - \mathrm{Re}\{(mc^2/e)[\xi_1(z)\vec{e}_1(z) + \xi_2(z)\vec{e}_2(z)]e^{-i\omega t}\}\,, \tag{56}$$

$$\vec{v} = \vec{v}_0 + \mathrm{Re}[\vec{V}(z)e^{-i\omega t}]\,, \tag{57}$$

$$\Phi = 0 + \mathrm{Re}[(mc^2/e)(\omega/kc)\xi_3 e^{-i\omega t}]\,, \tag{58}$$

$$\gamma = \gamma_0 + \mathrm{Re}(\Gamma e^{-i\omega t})\,, \tag{59}$$

$$N = N_0 + \mathrm{Re}(N_1 e^{-i\omega t})\,. \tag{60}$$

Then (29) and (30) yield on linearization

$$\left(-i\omega + u\frac{d}{dz}\right)(\gamma_0 V_1 + c\xi_1) - k_0\mu(\Gamma w + \gamma_0 V_2 + c\xi_2) - k_0 V_3(\gamma_0 w - c\xi_0) = -\Omega V_2 \tag{61}$$

$$\left(-i\omega + \frac{ud}{dz}\right)(\Gamma w + \gamma_0 V_2 + c\xi_2) + k_0\mu(\gamma_0 V_1 + c\xi_1) = \Omega V_1\,.$$

Rather than use (31) it is convenient to employ the linearized version of (4) which yields

$$\left(-i\omega + \frac{ud}{dz}\right)\Gamma = \left(\frac{\omega u}{kc}\right)\frac{d\xi_3}{dz} + \frac{i\omega w \xi_2}{c}\,. \tag{62}$$

Linearization of (1) gives

$$\left(-i\omega+\frac{ud}{dz}\right)N_1+\left(\frac{d}{dz}\right)(N_0V_3)=0\,, \tag{63}$$

while linearization of (3) implies

$$\Gamma/\gamma_0^3=(uV_3+wV_2)/c^2\,. \tag{64}$$

Equations (15) and (16) on using (27) yield

$$\frac{d^2\xi_1}{dz^2}-k_0^2\xi_1-2k_0\frac{d\xi_2}{dz}+\frac{\omega^2\xi_1}{c^2}=-\frac{\omega_p^2V_1}{c^3}\,, \tag{65}$$

$$\frac{d^2\xi_2}{dz^2}-k_0^2\xi_2+2k_0\frac{d\xi_1}{dz}+\frac{\omega^2\xi_2}{c^2}=-\left(\frac{\omega_p^2}{c^3}\right)\left(V_2+\frac{N_1w}{N_0}\right), \tag{66}$$

$$\frac{\omega}{kc}\frac{d^2\xi_3}{dz^2}=\frac{\omega_p^2}{c^2}\frac{N_1}{N_0}\,. \tag{67}$$

Note that Eqs. (60)–(67) are a system of eight linear ordinary differential equations with constant coefficients for the eight quantities V_1, V_2, V_3, Γ, N_1, ξ_1, ξ_2, and ξ_3. Thus we may seek solutions where all these scalars vary with z as e^{ikz}. If we write

$$\vec{\mathrm{E}}=\mathrm{Re}[\vec{\tilde{a}}(z)e^{i\omega t}]\,, \tag{68}$$

then it follows from (6) that

$$\vec{\tilde{a}}=-i(mc\omega/e)\vec{\xi}\,. \tag{69}$$

Equations (60) through (67) then imply

$$i(ku-\omega)(\gamma_0V_1+c\xi_1)-(k_0u-\Omega/\gamma_0)(\gamma_0V_2+c\xi_2+\Gamma w)$$
$$=(\Omega/\gamma_0)c\xi_2+(\Omega/\gamma_0)\Gamma w+k_0V_3(\gamma_0w-c\xi_0)\,, \tag{70}$$

$$(k_0u-\Omega/\gamma_0)(\gamma_0V_1+c\xi_1)$$
$$+i(ku-\omega)(\gamma_0V_2+c\xi_2+\Gamma w)=-(\Omega/\gamma_0)c\xi_1\,, \tag{71}$$

$$\Gamma=\frac{\omega}{c}\,\frac{u\xi_3+w\xi_2}{ku-\omega}\,, \tag{72}$$

$$\frac{N_1}{N_0}=-\frac{kV_3}{ku-\omega}\,, \tag{73}$$

$$\Gamma=(\gamma_0^3/c^2)(uV_3+wV_2)\,, \tag{74}$$

$$[1-c^2(k_0^2+k^2)/\omega^2]\xi_1-(2ik_0kc^2/\omega^2)\xi_2$$
$$=-(\omega_p^2/\omega^2)(V_1/c)\,, \tag{75}$$

$$(2ik_0kc^2/\omega^2)\xi_1+[1-c^2(k_0^2+k^2)/\omega^2]\xi_2$$
$$=-(\omega_p^2/\omega^2)[(V_2/c)+(w/c)(N_1/N_0)\,, \tag{76}$$

$$N_1/N_0=-(kc\omega/\omega_p^2)\xi_3\,. \tag{77}$$

It is convenient to express Γ, N_1, V_1, V_2, and V_3 in terms of ξ_1, ξ_2, and ξ_3. The result can be represented in the form

$$\underline{\epsilon}\cdot\vec{\xi}=0\,, \tag{78}$$

where the dielectric tensor

$$\underline{\epsilon}=\underline{\theta}+(\omega_p^2\tau/\gamma_0\omega^2)\underline{\psi} \tag{79}$$

and

$$\tau=(\Omega/\gamma_0)[(ku-\omega)^2-(k_0u-\Omega/\gamma_0)^2]^{-1}\,. \tag{80}$$

The components of θ are

$$\begin{aligned}
\theta_{11}&=1-c^2(k_0^2+k^2)/\omega^2-\omega_p^2/\gamma_0\omega^2\,,\\
\theta_{13}&=\theta_{31}=0\,,\\
\theta_{12}&=-\theta_{21}=-2ic^2k_0k/\omega^2\,,\\
\theta_{22}&=1-c^2(k_0^2+k^2)/\omega^2\\
&\quad-(\omega_p^2/\gamma_0\omega^2)[1+(u^2/c^2)(k^2c^2-\omega^2)(ku-\omega)^{-2}]\,,\\
\theta_{23}&=\theta_{32}=-(\omega_p^2/\gamma_0)(ku-\omega)^{-2}(w/\omega)(k-\omega u/c^2)\,,\\
\theta_{33}&=1-(\omega_p^2/\gamma_0)(ku-\omega)^{-2}(1-u^2/c^2)\,.
\end{aligned} \tag{81}$$

The elements of $\underline{\psi}$ are

$$\begin{aligned}
\psi_{11}&=k_0u-\Omega/\gamma_0\,,\\
\psi_{12}&=-i(ku-\omega)\left(1+\frac{w^2}{c^2}\,\frac{\omega}{ku-\omega}\right),\\
\psi_{13}&=-i(ku-\omega)\left(\frac{uw}{c^2}\,\frac{\omega}{ku-\omega}+\frac{\xi_0k_0c\omega}{\omega_p^2}\,\frac{ku-\omega}{k_0u-\Omega/\gamma_0}\right),\\
\psi_{21}&=i\left(\frac{k(u^2+w^2)}{u}-\omega\right),\\
\psi_{22}&=\left(\frac{k(u^2+w^2)}{u}-\omega\right)\frac{k_0u-\Omega/\gamma_0}{ku-\omega}\left(1+\frac{w^2}{c^2}\,\frac{\omega}{ku-\omega}\right),\\
\zeta_{23}&=\left(\frac{k(u^2+w^2)}{u}-\omega\right)\frac{k_0u-\Omega/\gamma_0}{ku-\omega}\\
&\quad\times\left(\frac{uw}{c^2}\,\frac{\omega}{ku-\omega}+\frac{\xi_0k_0c\omega}{\omega_p^2}\,\frac{ku-\omega}{k_0u-\Omega/\gamma_0}\right),\\
\psi_{31}&=i\omega w/u\,,\\
\psi_{32}&=\frac{\omega w}{u}\,\frac{k_0u-\Omega/\gamma_0}{ku-\omega}\left(1+\frac{w^2}{c^2}\,\frac{\omega}{ku-\omega}\right),\\
\psi_{33}&=\frac{\omega w}{u}\,\frac{k_0u-\Omega/\gamma_0}{ku-\omega}\left(\frac{uw}{c^2}\,\frac{\omega}{ku-\omega}+\frac{\xi_0k_0c\omega}{\omega_p^2}\,\frac{ku-\omega}{k_0u-\Omega/\gamma_0}\right).
\end{aligned} \tag{82}$$

In the limit $\Omega\to0$, τ vanishes and $\underline{\epsilon}$ reduces to $\underline{\theta}$, which apart from notation is the form found by Bernstein and Hirshfield.[1]

VI. THE DISPERSION RELATION AND NUMERICAL EXAMPLES

In order that (78) have nontrivial solutions it is necessary that the determinant

$$D=\det\underline{\epsilon}=0\,. \tag{83}$$

This yields an eighth-order polynomial equation for k. In practice, for the cases of interest $\omega_p^2 \ll \omega^2$ and $u\sim c$, and two of the roots are such that $\omega/k\approx-c$. That is, they propagate in the negative-z direction counter to the beam and are substantially unaffected by the tenuous beam. The remain-

ing six roots correspond to waves which propagate along the beam. When $\Omega \to 0$ the two of these which can be associated with cyclotron waves in the limit of no helical pump disappear, and one recovers the result of Bernstein and Hirshfield.[1] These features will be illustrated later when numerical examples are discussed.

Now Eqs. (61)–(67) comprise a tenth-order system of linear ordinary differential equations which require for a unique solution the stipulation of ten boundary conditions. Since usually there is negligible reflection of waves at the output end of an FEL amplifier of finite length, two conditions are the requirement that the amplitudes of the waves propagating counter to the beam be zero. This requirement can be most easily dealt with via solving the system of ordinary differential equations by means of a Laplace transform in z, as was done in Ref. 1, instead of the normal mode analysis. The dispersion relation, of course, determines the poles of the transform in terms of which the inversion can be readily accomplished. The resulting solution for $\tilde{a}(z)$ can be written in terms $\tilde{a}(0)$, assuming that all other first-order quantities are zero at $z=0$ and involve linear combinations of the six modes corresponding to the six roots with $\mathrm{Re}k>0$. Since in general these roots are nondegenerate, but differ by amounts of order Δk much less than ω/c, there will be interference amongst their contributions to $\tilde{a}(z)$, which becomes evident after a distance of order $2\pi/\Delta k$. This feature has been examined in detail in Ref. 1. We will not pursue it further here, other than to note that the single particle theory in which one examines the second-order energy change in a distance z of an electron moving in the zero- and first-order electromagnetic field, and identifies this with the gain in energy of the high frequency field, is valid only for $z\Delta k<1$.

We now consider the dispersion relation (83) in an FEL with guide magnetic field. Because of the complexity of the dielectric tensor $\underline{\epsilon}$ [see Eq. (79)] it is convenient to study the dispersion relation by comparing two FEL's, identical except that one has an axial field while the second does not and thus is characterized by the dispersion relation $D_0=\det(\underline{\theta})=0$, the properties of which are well understood. We make the comparison between the two lasers by fixing the parameters of the FEL without the guide field and adjusting the value of the pump field parameter ξ_0 in the laser with the guide field so that the axial velocities u (and therefore also w) in both lasers are identical. This assures the same Doppler upshift of the frequencies in the lasers. A similar comparison has been made by Friedland and Hirshfield for the single particle model of FEL.[3]

Let ξ_0^0 be the pump field parameter in the FEL without the guide field. The unperturbed electron velocity components are then given by $w/c=\xi_0^0/\gamma_0$ and $u/c=[1-(1+\xi_0^0)/\gamma_0^2]^{1/2}$. Therefore, following Eq. (35), with the guide field

$$\xi_0=\xi_0^0\left(1-\frac{\Omega}{\gamma_0 k_0 u}\right). \tag{84}$$

This equation demonstrates the intriguing possibility of reduction of the pump field in an FEL as one approaches the cyclotron resonance condition $\Omega/\gamma_0 - k_0 u$. Accessibility of the resonance, however, is not guaranteed, as was shown in the recent study[2] of the unperturbed electron beam orbits in an FEL with the guide field. It was demonstrated that for given values of γ_0, k_0, ξ_0, and Ω the electrons can possess more than one steady state. For example, Fig. 1 shows u/c versus Ω/c for $k_0=6\ \mathrm{cm}^{-1}$, $\gamma_0=3$, and $\xi_0=0.5$. For $\Omega>\Omega_{cr}$ it is seen that only one branch exists (branch C). But when $\Omega<\Omega_{cr}$ two additional branches (A and B) are allowed. It was also shown that the necessary condition for orbital stability of the steady-state solutions against small perturbations is given by the inequality

$$\frac{\Omega}{ck_0\xi_0}\left(\frac{w}{u}\right)^3<1. \tag{85}$$

Branch C is always stable, since $w<0$ on this branch. On branches A and B, $w>0$, but, as was shown, only branch A satisfied (85) and thus may be used in applications. Since the ratio w/u is kept constant in our comparative study, one can substitute the expression for ξ_0 found from (35) into (85) and write the stability condition in the following form:

$$\Omega<\Omega_{cr}=\frac{\gamma_0 k_0 u}{1+(w/u)^2}, \tag{86}$$

valid for branches A and B. In our sample case ($\gamma_0=3$, $k_0=6\ \mathrm{cm}^{-1}$, and $\xi_0^0=0.5$) one has $\Omega_{cr}/c=16.18\ \mathrm{cm}^{-1}$, and, therefore, according to (84),

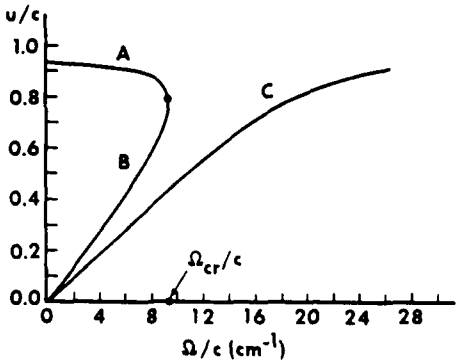

FIG. 1. Steady-state normalized axial velocity u/c as a function of normalized axial magnetic field Ω/c.

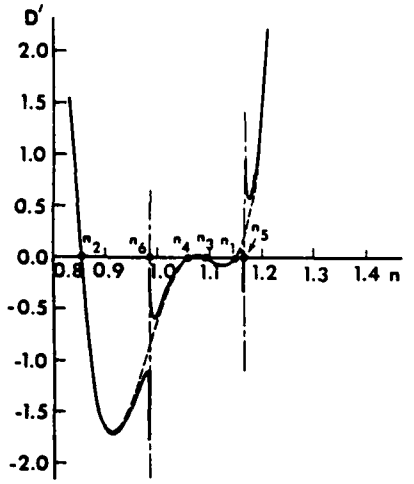

FIG. 2. Dispersion function D' on branch A for the case $\gamma_0=3$, $k_0=6\ \mathrm{cm}^{-1}$, and $\omega/c=40\ \mathrm{cm}^{-1}$. The dashed curve represents the FEL without the guide magnetic field and $\xi_0^0=0.5$. The solid curve is for the FEL with the guide field ($\Omega/c=6.5\ \mathrm{cm}^{-1}$), where smaller values of ξ_0^0 are used so as to provide the same values of u and w as for the dashed curve.

ξ_0 on branch A cannot become less than $\xi_{cr}=1.562\times10^{-2}$.

We return now to the study of the dispersion relation (83). The form of the dielectric tensor $\underline{\epsilon}$ [Eq. (79)] suggests that for values of ω_p small enough, the function D will differ significantly from D_0 only in the regions where $(ku-\omega)^2-(k_0u-\Omega/\gamma_0)^2\simeq 0$, as a result of the resonance in the denominator in τ [see Eq. (80)]. We demonstrate a typical effect of the axial guide field on the dispersion function D in Fig. 2, where the function $D'=D[ku-\omega)/\omega_p(1-u^2/c^2)]^2/\gamma_0$ (the full line) is shown versus $n=ck/\omega$ for branch A in the sample case when $\omega/c=40\ \mathrm{cm}^{-1}$, $\omega_p^2/c^2=0.5\ \mathrm{cm}^{-2}$, and $\Omega/c=6.5\ \mathrm{cm}^{-1}$. In the same figure the dashed line represents the case with no guide field.

It is well known[1] that the unstable regime in an FEL without the guide field can be described as a coupling between the transverse electromagnetic modes with the dispersion relation $n_{1,2}=1\pm ck_0/\omega$ and the electrostatic beam modes characterized by $n_{3,4}=c/u\pm c\omega_p/\gamma_0\omega u$. One can see from Fig. 2 that these four roots are only slightly perturbed by the presence of the axial field. There exist, however, two additional roots in the neighborhood of the resonance points $n_{5,6}=c/u\pm(ck_0/\omega-\Omega c/\gamma u\omega)$. If the resonances are widely separated as in the case of Fig. 2, the onset of the unstable mode is roughly the same as without the guide field, namely, as the frequency ω increases, the root n_1 moves to 1, passing the region $n_4<n<n_3$ (since $n_{3,4}\to c/u$). The modes couple in this region,

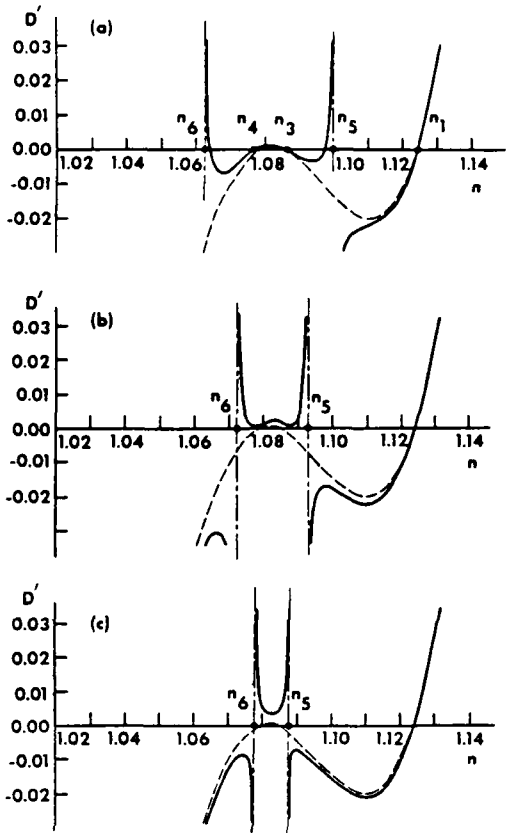

FIG. 3. Graphical representation of the dispersion function on branch A for the case $\gamma_0=3$, $k_0=6\ \mathrm{cm}^{-1}$, $\xi_0^0=0.5$, $\omega/c=50\ \mathrm{cm}^{-1}$, and increasing values of the guide field (the solid curves): (a) $\Omega/c=14\ \mathrm{cm}^{-1}$, (b) $\Omega/c=15\ \mathrm{cm}^{-1}$, (c) $\Omega/c=16\ \mathrm{cm}^{-1}$. The dashed curves correspond to the FEL without the guide field. Two pairs of roots of the dispersion relation become complex as the real roots n_3 and n_4 are squeezed by the resonances at n_5 and n_6.

and the roots of the dispersion relation are complex. When ω continues to increase, n_1 becomes less than n_4, the coupling diminishes, and one again has a stable regime.

New effects may occur when the resonances $n_{5,6}$ approach each other. This situation is shown in Fig. 3, where the full line represents the dispersion function on branch A for increasing values of Ω. One can see in this example that even for $\omega/c=50\ \mathrm{cm}^{-1}$ in our sample case (all the modes are stable in this case if $\Omega=0$) it is possible just by changing Ω to squeeze the roots $n_{3,4}$ by the resonances $n_{5,6}$ so that two pairs of the roots become complex. For higher frequencies, when again the FEL without the guide field is stable ($n_1<n_4$) one can also get an unstable regime as is demonstrated in Fig. 4 for $\omega/c=100\ \mathrm{cm}^{-1}$. Our numerical study

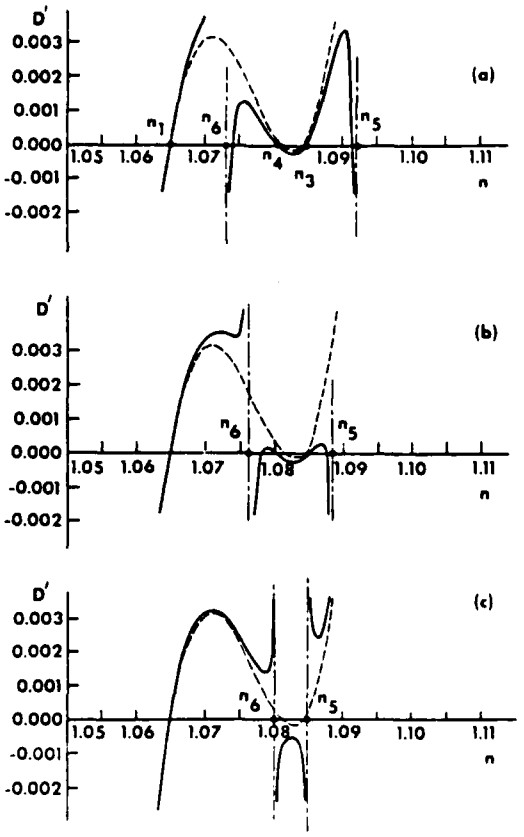

FIG. 4. Graphical representation of the dispersion function on branch A for the case $\gamma_0=3$, $k_0=6$ cm^{-1}, $\xi_0^0=0.5$, $\omega/c=100$ cm^{-1}. The solid curves: (a) $\Omega/c=14$ cm^{-1}; (b) $\Omega/c=15$ cm^{-1}; (c) $\Omega/c=16$ cm^{-1}. The dashed curves correspond to the FEL without the guide field.

shows that similar behavior is also characteristic for branch C with the only difference that there is only one pair of unstable modes in the low and the high frequency ranges, respectively.

We finally summarize our comparison of the FEL's with and without the guide field in Figs. 5 and 6, where the imaginary part of k is shown as a function of ω/c for various values of the axial field in our sample case ($\gamma_0=3$, $k_0=6$ cm^{-1}, $\xi_0^0=0.5$, $\omega_p^2/c^2=0.5$ cm^2). Figure 5 is for $0<\Omega/c<14.5$ cm^{-1} on branch A (the full lines) and $21<\Omega/c<28$ cm^{-1} on branch C (the dashed lines). The resonances $n_{5,6}$ are relatively wide apart from each other and formally the instability in this range of Ω occurs similarly to the case of the laser without the guide field. Nevertheless, the presence of the guide field increases the instability on branch A and tends to decrease it on branch C. In addition, the linewidth of the unstable regime is seen to be significantly increased at lower frequencies on branch A. Together with this, no instability exists at frequencies higher than those

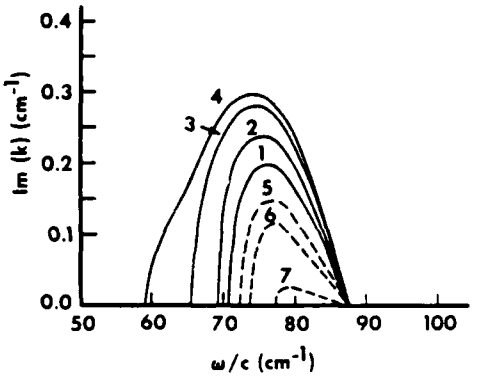

FIG. 5. Spacial growth rates Im(k) versus ω/c on branch A (solid curves) and C (dashed curves) for various values of Ω/c: (1) $\Omega/c=0$, (2) $\Omega/c=12$ cm^{-1}, (3) $\Omega/c=14$ cm^{-1}, (4) $\Omega/c=14.5$ cm^{-1}, (5) $\Omega/c=28$ cm^{-1}, (6) $\Omega/c=23$ cm^{-1}, (7) $\Omega/c=21$ cm^{-1}. For all the cases $\gamma_0=3$, $k_0=6$ cm^{-1}, and $\xi_0^0=0.5$.

characteristic of the FEL without the guide field. As one approaches the resonance condition $\Omega=\gamma_0 u k_0$ (further increasing Ω on branch A or decreasing it on branch C) a completely different type of behavior is observed as is shown in Fig. 6 for $\Omega/c=15.25$ cm^{-1} on branch A (the full line) and $\Omega/c=18$ cm^{-1} on branch C (the dashed line). The unstable region extends over the entire low-frequency range and there are two different unstable modes on branch A, as was mentioned previously. In addition there exist unstable modes in the high-frequency region, which was totally stable before. Note that the values of Imk in this high-frequency regime are only weakly dependent on the frequency itself.

Thus, in conclusion, we have demonstrated in

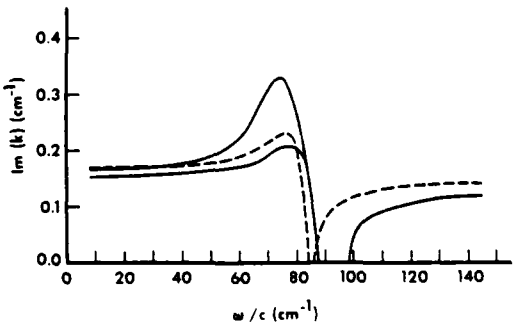

FIG. 6. Spatial growth rates Im(k) in the sample case ($\gamma_0=3$, $k_0=6$ cm^{-1}, $\xi_0^0=0.5$) versus ω/c in the regime, where the cyclotron modes couple to the beam modes (see Figs. 3,4). Branch A (solid curves): $\Omega/c=15.25$ cm^{-1}. Branch C (dashed curves): $\Omega/c=18$ cm^{-1}. The unstable modes are extended over the low- and high-frequency regions. There exist two different growth constants in this regime on branch A.

our numerical examples that the presence of the guide field in an FEL introduces the following desirable features:

(i) One can operate the laser with much lower magnitudes of the pump field without sacrificing the undulatory velocity of the electrons. This allows one to use shorter periods of the wiggler with the same currents.

(ii) The laser can be operated in higher gain regime by approaching the resonance condition $\Omega = k_0 v_{z0}$.

(iii) The linewidth of the unstable modes can be widely extended to both low- and high-frequency ranges.

ACKNOWLEDGMENT

This work was supported by the Office of Naval Research and by the National Science Foundation.

[1]I. B. Bernstein and J. L. Hirshfield, Phys. Rev. A 20, 1661 (1979).
[2]L. Friedland, Phys. Fluids 23, 2376 (1980).
[3]L. Friedland and J. L. Hirshfield, Phys. Rev. Lett. 44, 1456 (1980).

International Journal of Infrared and Millimeter Waves,
to be published in September 1981.

ORBIT STABILITY IN FREE ELECTRON LASERS*

P. Avivi, F. Dothan, A. Fruchtman,
A. Ljudmirsky, and J. L. Hirshfield+

Center for Plasma Physics
Hebrew University
Jerusalem, Israel

Helical magnetic wigglers for free electron lasers can produce non-helical electron trajectories if a uniform axial guide magnetic field is imposed. Freidland's necessary criterion for the existance of helical orbits is reviewed and shown to apply for non-relativistic electron energies. An experiment designed to test this criterion is described and results are compared with theory.

Key words: free electron laser, magnetic wiggler, electron orbits.

Introduction

Considerable effort is currently underway in the analysis (1), design (2), and construction (3) of free electron lasers for amplification of infrared and far infrared radiation. A typical device comprises a good quality electron beam with energy of 10's of MeV which moves through a periodic static pump magnetic field, termed a magnetic wiggler. Radiation propagating along the electron beam has been shown experimentally (4) to be amplified, but the single-pass small-signal gain may be quite small (7% was reported for a 520 cm length at λ = 10.6μ in Ref. 4).

Suggestions for enhancing the small-signal gain by superposing a uniform axial magnetic upon the wiggler field have appeared, based upon both single-particle (5,6) and collective (7) models. The gain enhancement can result from either increased equilibrium undulatory momentum (5), or from dynamical resonance between induced electromagnetic perturbations and the natural oscillations of electrons on helical orbits (6,7). The increased undulatory momentum results in a decreased axial momentum, and thus a decreased Doppler up-shift, i.e. the laser output frequency is shifted to longer wavelength. Gain enhancement may still be achieved without this wavelength increase by operating the device with a reduced wiggler field.

A necessary condition for achievement of the gain enhancement is that the equilibrium electron orbits in the wiggler be nearly helical. Without the axial guide field a helical magnetic wiggler produces a helical orbit; this result follows from the constancy of canonical angular momentum. But when the axial guide field is present, the orbits are generally not helical (8). They can be arranged to be nearly helical if the entry conditions into the wiggler are suitably tailored, and if the wiggler and guide field parameters are in a regime of stability, determined from the orbit parameters (9).

In this paper, we shall review the basis underlying the criterion for orbit stability, and shall present results of an experiment designed to test this criterion quantitatively.

Orbit Stability

Here we summarize (8) some aspects of the dynamics of charged particles moving in a static magnetic field given by

$$\begin{aligned} \underline{B}(z) &= \hat{e}_z B_o + (\hat{e}_x \cos k_o z + \hat{e}_y \sin k_o z) B_\perp \\ &= \hat{e}_3 B_o - \hat{e}_2 B_\perp \quad . \end{aligned} \tag{1}$$

Here B_o is the magnitude of the uniform axial guide field, and $B_\perp$ is the magnitude of the transverse helical field with pitch $\ell_o = 2\pi/k_o$. It has been shown (1) that the

charged particle dynamics in this field are described compactly if a coordinate system with basis vectors ($\hat{e}_1$, $\hat{e}_2$, $\hat{e}_3$) is used, rather than the Cartesian system ($\hat{e}_x$, $\hat{e}_y$, $\hat{e}_z$). The coordinate transformations follow from the definitions of $\hat{e}_2$ and $\hat{e}_3$ given in Eq. (1), and by $\hat{e}_1 = \hat{e}_2 \times \hat{e}_3$.

Of course, the field given by Eq. (1) does not satisfy $\nabla \times \underline{B} = 0$; it is however a good approximation to the actual field near the axis of two identical interspersed helical conductors carrying currents in opposite directions. The exact field, and the precise nature of the approximations leading to Eq. (1) will be discussed in a forthcoming paper (10).

For a particle of charge e, rest mass m, and relativistic energy factor γ, the steady-state solutions of the equation of motion $md(\gamma\underline{v})/dt = -e\underline{v} \times \underline{B}$ [with $\underline{B}$ given by Eq. (1)] are

$$u_1 = 0$$

$$u_2 = \frac{k_o \xi u_3}{k_o u_3 \gamma - \Omega/c} \qquad (2)$$

$$u_3 = (1 - u_2^2 - \gamma^{-2})^{1/2}$$

where $\underline{u} = \underline{v}/c$, $\Omega = eB_o/m$, and $\xi = eB_\perp/k_o mc$. These components correspond to ideal helical trajectories, since u_2 and u_3 are constants. However, these steady-state values can only be approached asymptotically, for an actual wiggler, because of coupling between the components in the transition region at the entrance to the wiggler (8), and because the form given by Eq. (1) is only an approximation.

The solutions given by Eq. (2) are depicted (for γ = 10.0, $k_o = 6.0\ cm^{-1}$, and $\xi = 1.0$) in Fig. 1. For $\Omega > \Omega_{cr}$ the equations are single-valued, whilst for $\Omega < \Omega_{cr}$ they are triple-valued. The critical axial guide field cyclotron frequency Ω_{cr} is given by

$$\Omega_{cr} = k_o c[(\gamma^2 - 1)^{1/3} - \xi^{2/3}]^{3/2} \quad . \qquad (3)$$

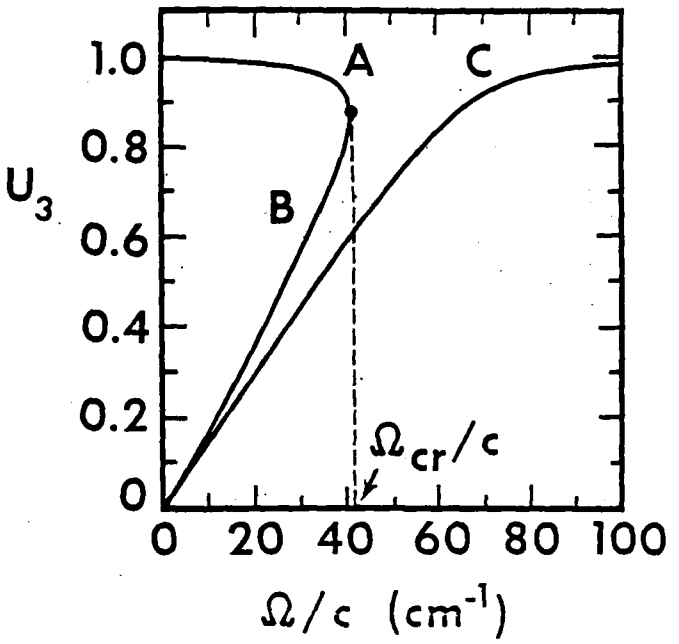

Figure 1. Solutions for steady-state axial momentum u_3, as a function of axial magnetic field, for $\gamma = 10$, $k_o = 6\ cm^{-1}$, and $\xi = 1$.

For smaller values of ξ than that chosen for Fig. 1, the curves hug more closely the asymptotes $u_3 = (1 - \gamma^{-2})^{1/2}$ and $u_3 = \Omega/k_o c\gamma$. Perturbation theory shows (8) that branches A and C in Fig. 1 are stable, whilst branch B is unstable. Thus, if a particle enters a wiggler along a gradually increasing guide field, it would move on a stable helical orbit along branch A, but at $\Omega = \Omega_{cr}$ the orbit would become unstable and thus severely non-helical. Examples of non-helical orbits are shown in Ref. 8. If Ω = const and the wiggler field increases gradually, a similar phenomenon occurs at ξ_{cr}, where

$$\xi_{cr} = [(\gamma^2 - 1)^{1/3} - (\Omega/k_o c)^{2/3}]^{3/2} , \qquad (4)$$

or $$(B_\perp/B_o)_{cr} = [(\gamma^2 - 1)^{1/3}(k_o c/\Omega)^{2/3} - 1]^{3/2} . \qquad (5)$$

Thus for a charged particle moving through a wiggler in a uniform axial guide field, the orbit can be nearly helical if $\xi < \xi_{cr}$ all along the wiggler but would depart significantly from helicity if $\xi > \xi_{cr}$.

Experiment

Although electron beams of interest for practical free electron lasers have relativistic energies, the phenomenon of helical orbit stability discussed above is not fundamentally a relativistic effect. Thus if the electron energy V is much less than 511 keV, so that we approximate $\gamma^2 - 1 \approx (2eV/mc^2)$, we can write Eq. (5) as

$$(B_\perp/B_o)_{cr} = [(8\pi^2 mV/eB_o^2 \ell_o^2)^{1/3} - 1]^{3/2}$$
$$= [(21.2V^{1/2}/B_o\ell_o)^{2/3} - 1]^{3/2} \qquad (6)$$

where, in the final expression, V is in volts, B_o is in gauss, and ℓ_o is in cm.

In the experiments to be described, electron beams in the energy range 4-14 keV were employed; a simple dc low-current ($\sim$ 10's of mA) crt electron gun could then be used to provide the electron beam with a diameter of about 1 mm and energy resolution of better than 1%. The helical wiggler, to be described more fully below, had a period ℓ_o = 3.6 cm. Thus, from Eq. (6), one sees that the transition from stable to unstable orbits would occur for very small wiggler fields indeed if the axial magnetic field were adjusted to be slightly above $5.89V^{1/2}$ gauss, i.e. in the range between 350 and 700 gauss. The axial magnetic field was in fact adjusted to dc values between about 300 to 3000 gauss. For a given electron energy V and axial field B_o the wiggler field amplitude $B_\perp$ was varied continuously in time by triggering a spark gap to discharge a capacitor in series with the wiggler coil. The ensuing RC-decay could be calibrated to give $B_\perp$ values as a function of time during each discharge pulse.

The wiggler coil itself was a bifilar periodic winding of 3 mm diam conductor would on a 53 mm diam cylinder with a uniform pitch of 36 mm. The uniform portion was 666 mm

long, i.e. 18.5 periods. At each end the wiggler diameter tapered outward to 100 mm over a 175 mm length. It was found that, in addition to provision of these tapered end portions, careful symmetrizing of the conductors at the end turns was essential for obtaining stable beam transmission through the wiggler. Furthermore, flux shunts at the ends were required to produce a smooth uniformly tapered transition into the wiggler. A plot of one component of the transverse field produced by this wiggler is shown in Fig. 2. (The uniform portion is not shown, as this portion is

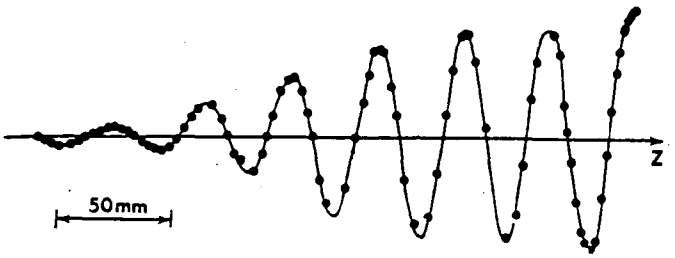

Figure 2. Measured transverse magnetic field at the entrance end of the wiggler.

relatively easy to produce.) This wiggler produced a field of about 20 gauss/kA, and fields up to 250 gauss have been routinely produced.

Several beam analyzers were constructed to examine the properties of the beam within the uniform portion of the wiggler. For the data to be presented in this paper, a movable analyzer was used consisting of two parallel plates spaced by 9 mm and positioned normal to the axial magnetic field. The first plate had a 3 mm hole in its center through which the beam would pass either in the absence of any wiggler field, or for wiggler field values below the critical value. In this case, paraxial helical orbits with diameter less than 3 mm were ascertained to be produced, so that the beam current was collected by the back plate. If the orbit were to involve excursions of more than 3 mm away from the axis, current would be collected by the front plate. When the beam was seen to migrate back and forth

between the two analyzer plates as the wiggler field decayed with time, this was taken as direct evidence for a strongly non-helical orbit. Two examples of this migration are shown in Fig. 3, which is traced from oscillograms of the

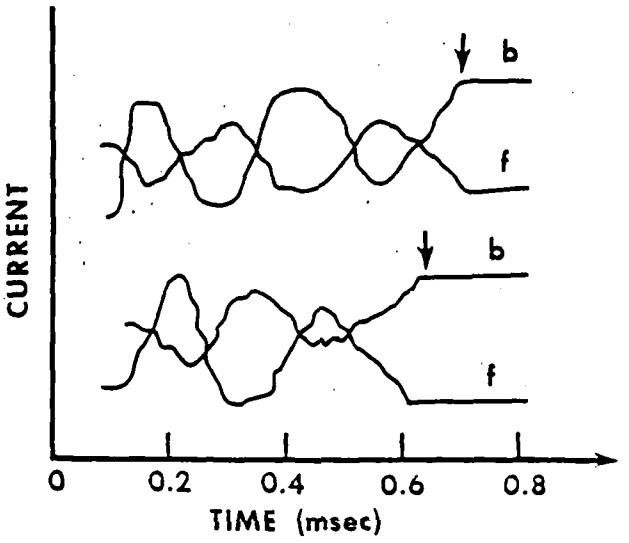

Figure 3. Measured currents to front (f) and back (b) plates of beam analyzer. Arrows indicate abrupt transitions from non-helical to helical orbits. Lower example is for a lower axial field value than upper example, so that transition occurs at higher value of wiggler field.

current waveforms to the analyzer plates as a function of time following firing of the wiggler field spark gap. The examples are for two different axial field values (lower for the bottom example than for the top). One sees the beam gyrate wildly back and forth between the two plates until a certain time, denoted by the arrows, when the wiggler field has decayed to a specific value. The transition to beam collection by the back plate alone (i.e. paraxial helical orbits) is seen to be abrupt. Values of wiggler field were noted at each transition point observed when axial field and beam energy were varied. These values are

plotted in Fig. 4 as a function of the independent variable

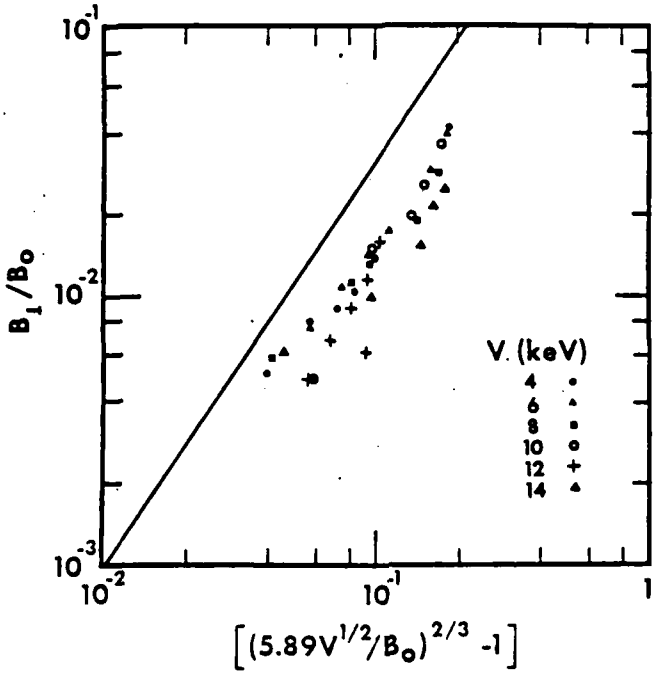

Figure 4. Measured values of $B_\perp/B_o$ at which transitions from stable to unstable orbits were observed, for electron energies between 4-14 keV. Solid line is theoretical prediction.

$(5.89V^{1/2}/B_o)^{2/3} - 1$, as suggested by Eq. (6) for ℓ_o = 3.6 cm. The straight line in Fig. 4 is this same variable raised to the three-halves power.

Transitions from stable to unstable orbits have been observed for wiggler fields as low as 2 gauss (lowest datum in Fig. 4).

Discussion

Magnetic wigglers for free electron laser applications produce helical electron orbits in the absence of an axial guide field, but may produce strongly non-helical orbits

if an axial field is present. One predicted (8) consequence of this phenomenon is an abrupt jump in the orbit from non-helical to helical once the magnetic wiggler field strength falls below a critical value, for fixed axial field and beam energy. This behavior has been observed experimentally over a wide range of (non-relativistic) beam energies and axial field strengths. The data follow an approximate three-halves power law in the variable $(8\pi^2 mV/eB_o^2 \ell_o^2 \gamma)^{1/3} - 1$, as suggested by the theory. The data fall systematically about 10-20% higher in this variable than is predicted (corresponding to about a factor-of-two smaller value of $B_\perp/B_o$ than is predicted). An overestimate in measured electron beam energies could explain the discrepancy between theory and experiment, but measurement accuracies are believed sufficient to rule this out. Finite geometry effects, due either to off-axis departures of the wiggler field from Eq. (1), or from the finite spatial resolution of the analyzer, could also contribute to the apparent discrepancy.

However, the crucial points for users of magnetic wigglers in axial guide magnetic fields are (1), the care required in wiggler construction (especially at the "first" turn, and within a gradual transition region) in order to observe a paraxial helical orbit at all; and (2), the clear observation of an abrupt transition between stable and unstable orbits at (sometimes very low) critical wiggler fields, much as had been predicted by theory.

It may be that the non-helical orbits will be of utility, although it would be easy to despair in attempting to formulate a theory for free electron laser operation with such a complex equilibrium state. These orbits can possess large amplitude harmonic overtones (10) which should radiate incoherent radiation at wavelengths a few time shorter than $\ell_o/2\gamma^2$. It may even be possible to observe coherent amplification on such a spatial overtone of the fundamental wiggler period; but speculation carries risks....

Acknowledgments

The authors have benefited from instructive discussions with L. Friedland. A critical reading of the manuscript by S. Y. Park is appreciated.

References and Footnotes

* This research was sponsored by the U.S. Office of Naval Research, and by the U.S.-Israel Binational Science Foundation.

† Also at Mason Laboratory, Yale University, P.O. Box 2159 Yale Station, New Haven, Connecticut 06520.

1. I. B. Bernstein and J. L. Hirshfield, Phys. Rev. A 20, 1661 (1979).

2. See, for example, C. A. Brau, Laser Focus 17, 48 (1981).

3. See, for example, E. D. Shaw and C. K. N. Patel, Workshop on Free-Electron Generators of Coherent Radiation, Telluride, Colorado, Aug. 1979.

4. D. A. G. Deacon, L. R. Elias, J. M. J. Madey, G. J. Ramien, H. A. Schwettman, and T. I. Smith, Phys. Rev. Lett. 38, 892 (1977).

5. P. Sprangle and V. L. Granatstein, Phys. Rev. A 17, 1792 (1978).

6. L. Friedland and J. L. Hirshfield, Phys. Rev. Lett. 44, 1456 (1980).

7. I. B. Bernstein and L. Friedland, Phys. Rev. A 23, 816 (1981).

8. L. Friedland, Phys. Fluids 23, 2376 (1980).

9. Of course, these considerations also to apply to other applications for wigglers in axial fields, such as in tailoring solid electron beams for gyrotrons.

10. S. Y. Park, J. M. Baird, R. A. Smith, and J. L. Hirshfield, to be published.

International Journal of Infrared and Millimeter Waves
To be published Sept. 1981.

DEGRADATION IN GAIN FOR A FREE ELECTRON LASER AMPLIFIER DUE TO ELECTRON MOMENTUM SPREAD*

A. Fruchtman and J. L. Hirshfield†

Center for Plasma Physics
and Racah Institute of Physics
Hebrew University of Jerusalem, Israel

A finite spread in axial momentum for the electron beam in a free electron laser amplifier is shown to decrease the small-signal gain. For millimeter and sub-millimeter wave amplifiers, where exponential growth dominates the gain, it is shown that the gain is approximately 3 db below that for a cold beam if the relative momentum spread $(\Delta u/u)_{1/2} = (G_o/248)^{1/2}(\lambda_o/L)$, where $G_o >> 1$ is the gain in db for the cold-beam case, λ_o is the magnetic wiggler period, and L is the amplifier length. Exact numerical examples are given for representative FEL amplifiers at 35 and 550 GHz.

Key words: free electron laser, amplifier, electron momentum spread.

Most theoretical work concerning amplification of radiation in free electron lasers (FELs) deals of necessity with idealized models. One idealization widely employed involves the neglect of finite momentum spread of the electron beam. The underlying mechanism for small-signal amplification involves axial synchronization in propagation velocity between one of the allowed modes of radiation supported by the beam, and the beam itself. Thus when a spread in axial beam momentum is present, a mixing-in-phase can be expected to degrade the amplification which would otherwise be predicted for a cold beam. Prior workers (1,2) have taken note of this fact and have provided estimates of the

effect of momentum spread. This paper presents an exact analytical model to account for finite momentum spread for a particular distribution function. When exponential growth dominates the gain, a simple approximate formula is derived to estimate the loss in gain due to the momentum spread. Exact numerical examples are also given for representative FEL amplifiers at 35 and 550 GHz.

The basic FEL model adopted here is identical to that treated by Bernstein and Hirshfield (B-H) (3). That work gave an exact small-signal solution of the Vlasov-Maxwell equations for the steady-state evolution of the co-propagating disturbance which grows in space on a relativistic electron beam passing along the axis of a helical magnetic wiggler. The B-H theory was derived for a beam of arbitrary momentum distribution in a wiggler of arbitrary strength, but the solutions presented were for the case of a cold beam, viz.,

$$f_o(\alpha,\beta,u) = N_o\delta(\alpha)\delta(\beta)\delta(u-U) \ . \qquad (1)$$

Here α and β are the two transverse components of canonical angular momentum $U_x - eA_x/mc^2$ and $U_y - eA_y/mc^2$, A_x and A_y are the components of the wiggler's vector potential, U_x and U_y are the transverse components of translational momentum, and $U = (\gamma^2 - 1)^{1/2}$ is the total momentum as related to the relativistic energy factor . (All momenta are normalized to mc.) Eq. (1) thus describes a beam which, prior to entering the wiggler, contains electrons possessing both zero transverse momentum and unique axial momentum U.

As mentioned above, an important source of degraded amplification is the finite spread of axial momentum on the electron beam. In the work reported here, we choose the simplest distribution capable of describing such a spread, viz.,

$$f_o(\alpha,\beta,u) = N_o\delta(\alpha)\delta(\beta)\left[\frac{H(u-U_1) - H(u-U_2)}{\Delta U}\right] , \qquad (2)$$

where $H(x) = 1$ for $x > 0$, $H(x) = 0$ for $x < 0$, and $\Delta U = U_2 - U_1 > 0$. This distribution can of course not be realized in nature [in the same sense that the distribution given by Eq. (1) cannot]. It may, however, not be a bad approximation for certain accelerators (except for the

sharp edges); but its utility here is that it enables an analytic form to be derived for the governing dispersion relation.

The goal of the present work is identical to that in B-H, namely to calculate the power gain G (in db) for a single pass of electromagnetic radiation along a FEL amplifier of length L.

$$10^{G/10} = a_2(L)a_2^*(L) - 1 \quad . \tag{3}$$

Here $a_2(L)$ is the dimensionless wave electric field at the amplifier output, normalized to unity at the input. The subscript "2" labels one of the three polarizations permitted, namely that which twists in space a quarter-period behind the wiggler's vector potential. [Eqs. (35) and (37) in B-H give the other two polarizations.]

The wave amplitude $a_2(L)$ is a superposition of several co-propagating normal modes, each with its wavenumber k_j, viz.,

$$a_2(L) = \sum_j \frac{B(k_j)}{R'(k_j)} \exp(ik_jL) \quad . \tag{4}$$

The relative mode amplitudes $B(k_j)/R'(k_j)$ are prescribed once boundary conditions are set. $R(k_j) = 0$ is the dispersion relation for the system which determines the $k_j(\omega)$, assuming $R^{-1}(k)$ to have simple poles. For the cold beam case $R(k_j)$ is a sixth-order polynomial.

$$\begin{aligned} R(x) = {} & [(x-\mu)^2 - \delta^2(1+\xi^2)][(x+x_o)^2 - b^2][(x-x_o)^2 - b^2] \\ & + \xi^2\delta^2(x^2-b^2)(x^2+x_o^2-b^2) \ , \end{aligned} \tag{5}$$

where $x = kc/\omega$, $x_o = k_oc/\omega$; $\delta = (\omega p/\omega)(U/\gamma U_z^3)^{1/2}$, $b = (1-U_z^2\delta^2)^{1/2}$, $\mu = \gamma/U_z$, $U_z = (U^2-\xi^2)^{1/2}$, and $\xi = -eB_o/mc^2k_o$. The wiggler field strength and wavenumber are B_o and k_o. This equation has been obtained as well by Sprangle (1), and related forms have been derived and discussed by Kroll and McMullin (2) and by Kwan, Dawson, and Lin (4). When $\delta << x_o << 1$, a reduced form of Eq. (5) is a good approximation, namely

$$R(x) \simeq [(x-\mu)^2 - \delta^2(1+\xi^2)][x - (b+x_o)] + \frac{1}{2}\xi^2\delta^2 x_o \ . \quad (6)$$

For $k_o/k \lesssim (1+\xi^2)/2\gamma^2$ the maximum growth occurs near $b+x_o - \mu = (\delta^2\xi^2 x_o/2)^{1/2}$. To requisite accuracy the roots are

$$\begin{aligned} x_1 &= \mu + (\delta^2\xi^2 x_o/2)^{1/3}\exp(-\pi i/3) \\ x_2 &= x_1^* \qquad (7) \\ x_3 &= \mu - (\delta^2\xi^2 x_o/2)^{1/3} \ . \end{aligned}$$

These roots are of use in scaling estimates when exponential gain is dominant. Exact numerical evaluations given in B-H show, however, that Eq. (7) cannot be used to determine the entire gain spectrum.

When Eq. (2) is employed as the distribution function all the momentum-space integrals in the Vlasov formulation can be expressed analytically. We then find

$$\begin{aligned} R(x) = [(x-\mu_1)(x-\mu_2) - \delta'^2(1+\xi^2)][(x+x_o)^2 - b'^2] \\ \times [(x-x_o)^2 - b'^2] + \xi^2\delta'^2(x^2-d^2)(x^2+x_o^2-b'^2) \ , \end{aligned} \quad (8)$$

where

$$\delta'^2 = -\frac{\omega_p^2}{\omega^2}\ \frac{1}{1+\xi^2}\ \frac{\Delta\mu}{\Delta U} \ ;$$

$$b'^2 = 1 - \frac{\omega_p^2}{\omega^2}\ \frac{1}{\Delta U}\ \ell n\left(\frac{\gamma_2 + U_{z2}}{\gamma_1 + U_{z1}}\right) \ ;$$

$$d^2 = 1 - \frac{1}{\Delta U}\ \frac{\omega_p^2}{\omega^2}\left[\Delta\mu - \frac{1+\xi^2}{\Delta\mu}\left(\frac{1}{U_{z1}} - \frac{1}{U_{z2}}\right)^2\right] \ ;$$

$\Delta\mu = \mu_2 - \mu_1 < 0$, $\gamma_{1,2}^2 = 1 + U_{1,2}^2$, $U_{z1,2}^2 = U_{1,2}^2 - \xi^2$, and $\mu_{1,2} = \gamma_{1,2}/U_{z1,2}$.

When $\Delta U/U \ll 1$, $\Delta\mu \simeq -U\Delta U(1+\xi^2)\gamma U_z^3$, $\delta' \simeq \delta$, and $b' \simeq d \simeq b$. Thus the only effect of finite momentum spread in this limit is in the factor $(x-\mu_1)(x-\mu_2) = (x-\bar{\mu})^2 - (\Delta\mu/2)^2$ in the first bracket in Eq. (8), where $\bar{\mu} = (\mu_1+\mu_2)/2$. The close similarity between Eqs. (8) and (5), and the simplicity of the former, make determination of the roots k_j a routine matter. This simplicity is not enjoyed when the momentum spread is described by functions $f_o(\alpha,\beta,U)$ with non-zero values of $\partial f_o/\partial U$ in a finite interval, because of wave-particle resonance effects.

As for the cold-beam case, where $\delta' \ll x_o \ll 1$, Eq. (8) may be reduced to the approximate form

$$R(x) \simeq [(x-\bar{\mu})^2 - (\Delta\mu/2)^2][x-(b'+x_o)] + \xi^2\delta'^2x_o/2 = 0. \quad (9)$$

If $(\Delta\mu/2)^2 \ll 3(\xi^2\delta'^2x_o/2)^{1/3}$, the roots of Eq. (9) near $b'+x_o-\bar{\mu} = (\xi^2\delta'^2x_o/2)^{1/2}$ are approximately

$$\begin{aligned} x_1 &= \bar{\mu} + (\xi^2\delta'^2x_o/2)^{1/3}\exp(i\pi/3) \\ &\quad + \tfrac{1}{3}(\Delta\mu/2)^2(\xi^2\delta'^2x_o/2)^{-1/3}\exp(-i\pi/3) \\ x_2 &= x_1^* \\ x_3 &= \bar{\mu} - (\xi^2\delta'^2x_o/2)^{1/3} - \tfrac{1}{3}(\Delta\mu/2)^2(\xi^2\delta'^2x_o/2)^{-1/3}. \end{aligned} \quad (10)$$

Thus the spatial growth constant $\mathrm{Im}x_1$ is seen to decrease on account of momentum spread as

$$\mathrm{Im}x_1 \simeq \frac{\sqrt{3}}{2}\left(\xi^2\delta'^2x_o/2\right)^{1/3}\left[1-\frac{1}{3}\left(\frac{\Delta\mu}{2}\right)^2\left(\xi^2\delta'^2x_o/2\right)^{-2/3}\right]. \quad (11)$$

For pure exponential gain, i.e. excluding the 15.6 db input coupling loss (see B-H), one has

$$G = 54.58(L/\lambda)\mathrm{Im}x_1 \quad \text{db} \quad (12)$$

where λ is the radiation wavelength. From Eq. (11) we can write $G = G_o - G_1$, where G_o is the gain with no momentum spread, and G_1 is the small decrease due to the spread

$$G_o = 54.58(L/\lambda)\frac{\sqrt{3}}{2}(\xi^2\delta^2 x_o/2)^{1/3} \text{ db} \quad . \qquad (13)$$

For $\xi = 0.47$, $\lambda = 4.9$, $x_o = 2.73 \times 10^{-2}$, $\delta^2 = 3.80 \times 10^{-6}$, and $L/\lambda = 367$ (corresponding to a representative FEL amplifier to be discussed below), Eq. (13) gives $G_o = 39.1$ db. [If one subtracts the 15.6 db input coupling loss, the actual gain would be 23.5 db (at a wavelength of 560 μm).] Now

$$G_1 = \frac{54.58}{8\sqrt{3}} \frac{L}{\lambda} (\Delta\mu)^2 (\frac{1}{2} \xi^2\delta^2 x_o)^{-1/3} \text{ db} \quad . \qquad (14)$$

Substituting from Eq. (13) gives the value of $\Delta\mu$ which would bring about a gain loss G_1

$$(\Delta\mu)^2 = 5.37 \times 10^{-3} G_o G_1 (\lambda/L)^2 \quad . \qquad (15)$$

For the example cited above with $L/\lambda = 367$ we find $\Delta\mu = 2.16 \times 10^{-3}$ for $G_o = 39.1$ db and $G_1 = 3$ db, i.e. for a factor-of-two decrease in power amplification. This corresponds to a relative momentum spread $\Delta U/U = |\Delta\mu|[\gamma U_z^3/U^2(1 + \xi^2)]$ of 0.041.

Equation (10) also suggests that the frequency at which gain has its peak value will decrease as momentum spread increases.

Exact numerical evaluations for small-signal gain G have been carried out using the full dispersion relation [Eq. (8)], and with amplitudes [see Eq. (4)] appropriate to a perfectly matched amplifier output. One example is for a mm-wave amplifier employing an electron beam typical of that produced by a small Febetron accelerator, with $\gamma = 1.78$, $J = 100$ A/cm^2, $\lambda_o = 3.6$ cm, $\xi = 0.2$, and $L = 36$ cm. Gain curves are shown in Fig. 1 for zero momentum spread, and for finite momentum spreads between 5 and 20%. Gain is seen to fall by one-half for $\Delta U/U \approx 0.15$, and the frequency for peak gain drops by about 6%. A second example is for a sub-mm wave amplifier employing a beam typical of the VEBA accelerator at Naval Research Laboratory, with $\gamma = 4.9$, $J = 6$ kA/cm^2, $\lambda_o = 2.0$ cm, $\xi = 0.47$, and $L = 20$ cm. For this case the computed gain curves are shown in Fig. 2, again for zero momentum spread and for spreads between 5 and 20%.

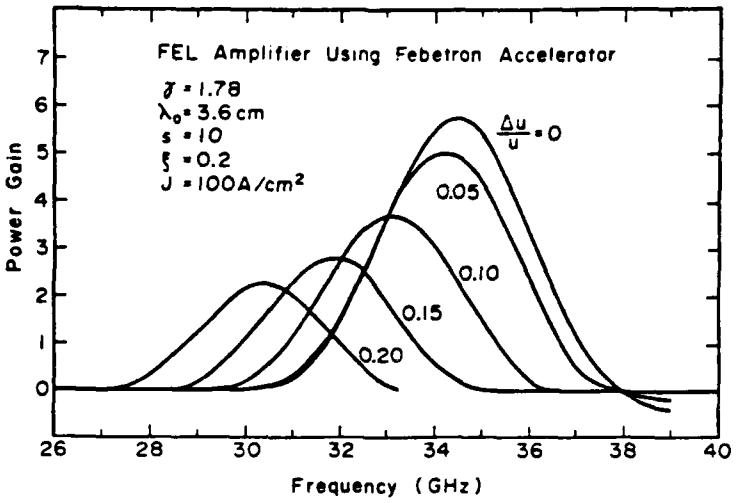

Figure 1. Gain curves for a FEL using a 400 kV electron beam, for electron momentum spread between 0 and 20%.

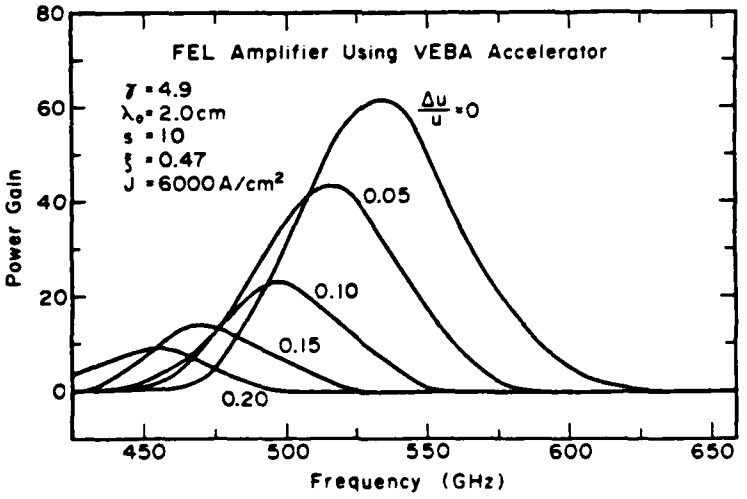

Figure 2. Gain curves for a FEL using a 2.0 MV electron beam, for electron momentum spread between 0 and 20%.

Comparisons between the exact results (Fig. 2) and the approximate predictions [Eqs. (12-15)] are instructive. The peak gain for the cold beam is 17.8 db (i.e. 60×) compared with the approximate value of 23.5 db. The gain drops by half to 14.8 db (i.e. 30×) for $\Delta U/U$ somewhat greater than 10%; our approximate result is 4.1%. These comparisons for the example presented in Fig. 1 are not meaningful since the peak gain G_o is less than 7.8 db (6×).

Finally, we point out the scaling laws suggested by Eqs. (12-15), valid for high gain devices where exponential growth dominates. For negligible momentum spread,

$$G_o \sim J^{1/3} L \xi^{2/3} \lambda^{-2/3} \lambda_o^{-1/3} \text{ db}$$

or equivalently (16)

$$G_o \sim J^{1/3} (L/\lambda_o) \xi^{2/3} \gamma^{4/3} \text{ db} \quad .$$

For the gain decrease $G_1 << G_o$ due to finite momentum spread we have

$$G_1 G_o \sim (\Delta U/U)^2 (L/\lambda_o)^2 \quad (\text{db})^2 \quad . \qquad (17)$$

Eq. (17) indicates that high gain short amplifiers are less susceptible to gain degradation due to momentum spread, than are low gain long amplifiers. This scaling is independent of λ and γ provided G_o is high. For $G_1 = 3$ db, the numerical value for Eq. (17) gives $(\Delta U/U)_{1/2} = (G_o/248)^{1/2} (\lambda_o/L)$, where $(\Delta U/U)_{1/2}$ is the relative momentum spread for a factor-of-two decrease in gain. Gain degradation for long-wiggler FELs operating in the collective regime can be expected to be serious unless $\Delta U/U << 1$.

It should be added as a caveat however that momentum spread may not always degrade gain in a FEL. The geometrical optics theory for a FEL amplifier (5) shows that gain may arise from a wave-particle resonance, provided $f_o(\alpha,\beta,u)$ is not symmetric in u about its maximum, and provided $\partial f_o/\partial u$ has the requisite sign at the wave's phase velocity. It is expected that this mechanism would compete with that discussed in the present paper, and could in fact allow substantial gain in the presence of tailored momentum spread.

Acknowledgment

Appreciation is extended to Dr. S. Y. Park for a critical reading of the manuscript.

References

* This research was sponsored by the U.S. Office of Naval Research, and by the U.S.-Israel Binational Science Foundation.

† Also at Mason Laboratory, Yale University, P.O. Box 2159, Yale Station, New Haven, Connecticut 06520.

1. P. Sprangle and R. A. Smith, Phys. Rev. A 21, 293 (1980).

2. N. M. Kroll and W. A. McMullen, Phys. Rev. A 17, 300 (1978).

3. I. B. Bernstein and J. L. Hirshfield, Phys. Rev. A 20, 1661 (1979).

4. T. Kwan, J. M. Dawson, and A. T. Lin, Phys. Fluids 20, 581 (1977).

5. I. B. Bernstein and J. L. Hirshfield, Phys. Rev. Lett. 40, 761 (1978).

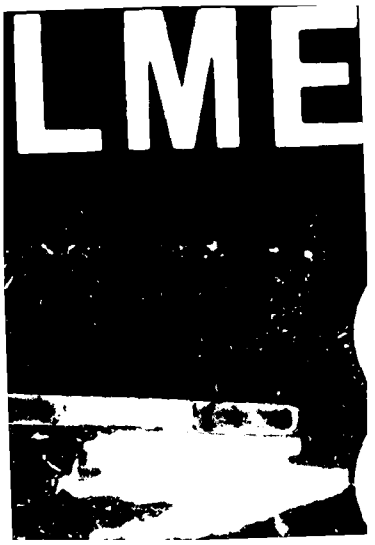
LME